

Nature and significance of small volume fall deposits at composite volcanoes: Insights from the October 14, 1974 Fuego eruption, Guatemala

W. I. Rose · S. Self · P. J. Murrow · C. Bonadonna ·
A. J. Durant · G. G. J. Ernst

Received: 7 January 2006 / Accepted: 31 October 2007
© Springer-Verlag 2007

Abstract The first of four successive pulses of the 1974 explosive eruption of Fuego volcano, Guatemala, produced a small volume ($\sim 0.02 \text{ km}^3$ DRE) basaltic sub-plinian tephra fall and flow deposit. Samples collected within 48 h after deposition over much of the dispersal area (7–80 km from the volcano) have been size analyzed down to 8ϕ ($4 \mu\text{m}$). Tephra along the dispersal axis were all well-sorted ($\sigma_\phi = 0.25\text{--}1.00$), and sorting increased whereas thickness and median grain size decreased systematically downwind. Skewness varied from slightly positive near the vent to

slightly negative in distal regions and is consistent with decoupling between coarse ejecta falling off the rising eruption column and fine ash falling off the windblown volcanic cloud advecting at the final level of rise. Less dense, vesicular coarse particles form a log normal sub-population when separated from the smaller ($\text{Md}_\phi < 3\phi$ or $< 0.125 \text{ mm}$), denser shard and crystal sub-population. A unimodal, relatively coarse ($\text{Md}_\phi = 0.58\phi$ or 0.7 mm $\sigma_\phi = 1.2$) initial grain size population is estimated for the whole (fall and flow) deposit. Only a small part of the fine-grained, thin 1974 Fuego tephra deposit has survived erosion to the present day. The initial October 14 pulse, with an estimated column height of 15 km above sea level, was a primary cause of a detectable perturbation in the northern hemisphere stratospheric aerosol layer in late 1974 to early 1975. Such small, sulfur-rich, explosive eruptions may substantially contribute to the overall stratospheric sulfur budget, yet leave only transient deposits, which have little chance of survival even in the recent geologic record. The fraction of finest particles ($\text{Md}_\phi = 4\text{--}8\phi$ or $4\text{--}63 \mu\text{m}$) in the Fuego tephra makes up a separate but minor size mode in the size distribution of samples around the margin of the deposit. A previously undocumented bimodal–unimodal–bimodal change in grain size distribution across the dispersal axis at 20 km downwind from the vent is best accounted for as the result of fallout dispersal of ash from a higher subplinian column and a lower “co-pf” cloud resulting from pyroclastic flows. In addition, there is a degree of asymmetry in the documented grain-size fallout pattern which is attributed to vertically veering wind direction and changing windspeeds, especially across the tropopause. The distribution of fine particles ($< 8 \mu\text{m}$ diameter) in the tephra deposit is asymmetrical, mainly along the N edge, with a small enrichment along the S edge. This pattern has hazard significance.

Editorial responsibility: H Delgado

W. I. Rose (✉) · A. J. Durant · G. G. J. Ernst
Dept. of Geological Engineering and Sciences,
Michigan Technological University,
Houghton MI 49931, USA
e-mail: raman@mtu.edu

S. Self
Volcano Dynamics Group, Dept. of Earth Sciences,
The Open University,
Milton Keynes MK7 6AA, UK

P. J. Murrow
Shinshu University,
Matsue, Japan

G. G. J. Ernst
Mercator & Ortelius Research Centre for Eruption Dynamics,
Geological Institute, Ghent University,
Ghent, Belgium

C. Bonadonna
University of South Florida,
Tampa, FL, USA

A. J. Durant
School of Geographical Sciences/Department of Earth Sciences,
University of Bristol,
Bristol BS8 1RJ, UK

Keywords Volcanic ash · Tephra · Subplinian · Vulcanian · Fallout · Guatemala · Fuego

Introduction

Since the first systematic descriptions of pyroclastic deposits in the early 1970s, many tephra deposits have been thought to result from so-called *vulcanian* eruptions. Vulcanian eruptions are named after Vulcano in Italy, a small volcano that produced a series of highly explosive eruptions in 1888–1890 which contained both trachytic and rhyolitic materials (Keller 1980). The name has been attached to many short-lived eruptions that produce grey or black tephra. Vulcanian activity produces thin, small volume ($<1 \text{ km}^3$) stratified tephra deposits which contain large ballistic blocks and bombs close to the vent, and, in spite of the rhyolitic composition of their namesake, are usually basaltic to andesitic in composition (Cas and Wright 1987; pp 153–156). They appear at first to have higher fragmentation indices than Plinian deposits, and uncertainty exists about the juvenile/non juvenile proportions and the

role of vaporization of groundwater in the mechanism of vulcanian explosions (Nairn and Self 1978; Fisher and Schminke 1983). Tephra deposits of vulcanian-type eruptions from intermediate composition stratovolcanoes have been well documented only at Soufrière Hills Volcano, Montserrat, where there is also uncertainty about whether some of the deposits are truly subplinian or vulcanian (e.g. 17 September 1996 eruption; Young et al. 1998). Whereas tephra deposits of Plinian, phreatoplinian, and strombolian eruptions are moderately well-understood with respect to their genesis, grain-size characteristics, transport, and deposition (see Cas and Wright 1987 for a summary), little work has been done on the fine-grained fallout from basaltic or andesitic subplinian/vulcanian activity. One outstanding reason for this is the impermanent nature of the fall deposits, which are generally small in volume and, especially in their distal portions, easily eroded (e.g. Self 1975; Bonadonna et al. 2002). They usually do not form a conspicuous part of the tephra stratigraphy preserved around composite volcanoes and, because of this, hazard assessment at tropical volcanoes based on the record of past eruptions is inherently incomplete and thus often inaccurate.

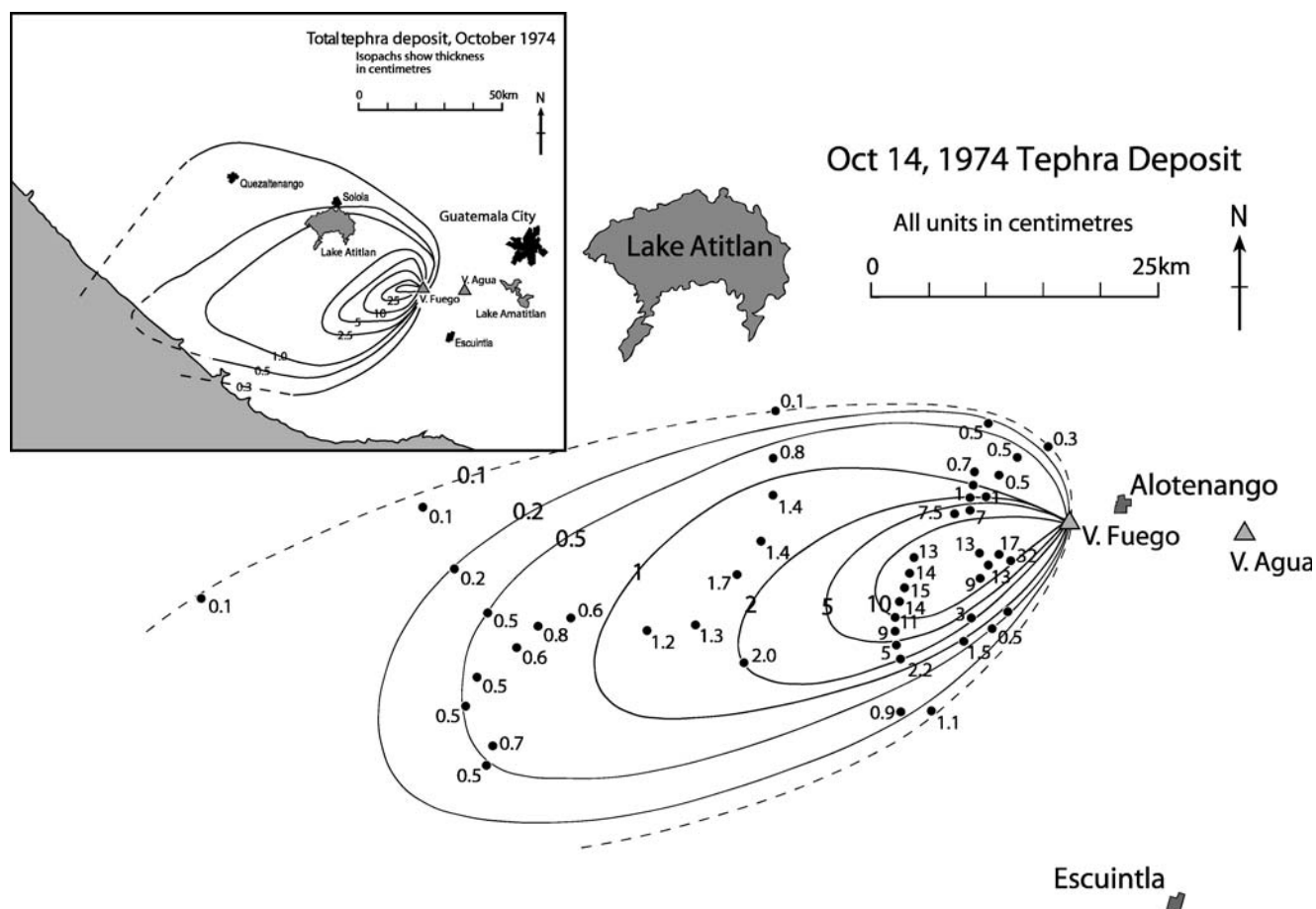


Fig. 1 Isopach map of October 14, 1974 scoria and tephra unit from Volcán de Fuego; individual location thicknesses (dots) and contours in cm. Inset (upper left) shows a map of the whole October 1974

tephra deposit (consisting of four fall units), giving only isopachs in cm (after Rose et al. 1978)

This study focuses on the Volcán de Fuego deposit of October 14, 1974 (Fig. 1), previously described as typical of fine-grained vulcanian tephra deposits (Murrow et al. 1980). It was deposited mostly upon land, was comprehensively mapped and sampled *immediately after* its eruption when it was extremely well preserved (Rose et al. 1978; Murrow et al. 1980), although now it is almost totally removed by erosion (W I Rose, unpublished data, 2005). We here present the results of size analyses of the October 14 deposit, their implications for eruption and depositional mechanisms, and a re-evaluation of eruption column heights.

Background and activity at Volcán de Fuego

Like many classifications of natural phenomena, the classification of eruption types is imperfect. According to Morrissey and Mastin (2000, p. 463), vulcanian eruptions are typically brief (lasting seconds to a few minutes) and the examples cited are all of small magnitude (typically $< 10^6 \text{ m}^3$, or $\sim 1 \times 10^{10} \text{ kg}$). However, vulcanian eruption columns may rise to 20 km height, and they are characterized by discrete, violent explosions. Subplinian activity is thought to represent a step up in mass ($\sim 10^{11} \text{ kg}$) and is associated with higher, more sustained (yet inherently non-steady in the vent) eruption columns (Cioni et al. 2000). The Fuego eruption has been termed *vulcanian* by Rose et al. (1978) but it is difficult to be adamant about this since the distinction between *vulcanian* and *subplinian* depends on whether the eruption is maintained or a series of distinct explosions of short duration. In practice, if explosions are quite closely spaced, the distinction is hard to judge. Indeed, McBirney (1973) recognized this dichotomy and proposed two end-member types of vulcanian activity: *cannon-like* (for discrete explosions) and *gas streaming* (for maintained activity). The Fuego eruption studied here could be described as a 5-h continuous event or as a 5-hour-long sequence of closely spaced (intervals of < 1 to 30 s) explosions. The gas thrust of the eruption was maintained but discrete explosions could sometimes be heard. Seismic records are not available. Due to the evidence presented below, we have now decided to characterize this deposit, and the eruption, as *subplinian*, in accordance with its sustained nature and physical characteristics, and evidence for this is presented below. Whatever its classification, the deposit is typical of activity of composite volcanoes like Fuego and our description here is aimed at better documentation of their common, easily-eroded, fine-grained tephra deposits that are not well preserved in the geological record.

The Fuego vent (Fig. 2) is a vertical conduit (see Rose et al. 1978 and Roggensack 2001 for discussion) which is sometimes plugged by lava that fills the summit crater and



Fig. 2 Oblique aerial photograph of the summit region of Fuego Volcano, 15 January 2003, looking N. Photo shows steep upper slopes of Fuego and its summit crater (3,763 m) which is the source vent of all recent eruptions. On the *left* and *behind* Fuego is Acatenango (3,976 m). USGS Photo by J Vallance

then flows down the steep barrancas (valleys) as lava flows. During lava flow eruptions without vertical explosions, Fuego's lavas may break up along the *barrancas* (flank valleys) and create block-and-ash flows. During explosive phases, such as on 14 October 1974, it is difficult to tell whether pyroclastic flows result from breakup of active flows or from partial collapse of the lower region of an eruption column, but the general character of the pyroclastic flows and deposits is like a block-and-ash flow. Davies et al. (1978) describe the H/L of the Fuego deposits as ~ 0.1 , like those produced from block-and-ash flows (Freundt et al. 2000), whereas fountain collapse pyroclastic flows usually have an H/L that is much lower. However, accompanying block-and-ash flows is a consistent characteristic of Fuego's explosive eruptions. Fuego's 1974 pyroclastic flows reached a maximum of 18 km from the summit crater (Davies et al. 1978).

During the past 450 years explosive eruptions of Fuego have emitted about 1.7 km^3 DRE ($\sim 4.7 \times 10^{12} \text{ kg}$) of high Al basalt in at least 60 summit eruptions (Martin and Rose 1981). Typically these yield small volume (usually $< 0.1 \text{ km}^3$ DRE) pyroclastic fall and flow deposits in events usually lasting a few hours. From a dynamic point of view, despite the pulsatory style of explosions in the vent, these eruptions are in fact quasi-steady in character. This is because the eruption duration is typically many times longer than the time required by the rising eruption column to reach its final level of rise and spread out (on the order of minutes, e. g. Sparks et al. 1997).

Fuego erupts porphyritic, water-rich, high-Al basalt (Harris and Anderson 1984; Sisson and Layne 1993) and was one of the first volcanoes recognized as releasing "excess sulfur" (Rose et al. 1982). The total range of composition for all Fuego lavas (Fig. 3) includes andesites, but all historic materials are basalts. Studies of the 1974

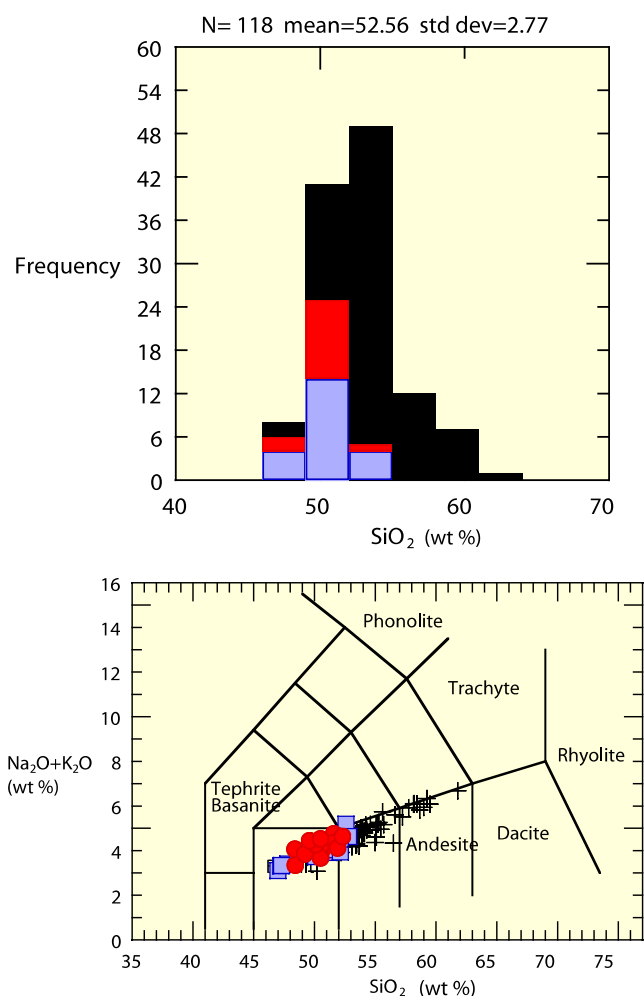


Fig. 3 Chemical composition of all analyzed erupted rocks from Fuego Volcano (118 total); spanning the entire age history. *Red* shows October 14, 1974 materials, *blue* shows other 1974 materials and *black* are the entire Fuego suite. In *upper diagram*, frequency is number of samples. *Lower diagram* superimposes the classification of LeBas et al. (1986), with only a few fields labelled for clarity; most 1974 Fuego materials are high alumina basalts. Data from CENTAM (Carr and Rose 1987) and unpublished data of W I Rose

tephra deposits suggest that the basalt underwent crystal fractionation within a vertical dike before eruption. The zoning patterns of plagioclase crystals and the timing of Fuego eruptions (including the 14 October 1974 event) likely reflect a tidal triggering mechanism (Martin and Rose 1981; Anderson 1984), consistent with pre-fragmentation level magma movements typical of low viscosity magmas, especially as the Fuego basaltic magmas are often extremely rich in dissolved volatiles (up to 6% water) lowering viscosity and that much of the high microcrystal content may form as a result of loss of these volatiles at the very latest stages of ascent. Melt inclusion studies show the 1974 eruption was of hybridized basalts from a variety of crustal levels (Roggensack 2001). Before the modern period, Fuego produced more silicic lavas (Chesner and Rose

1984; Chesner and Halsor 1997) and the Fuego complex may have experienced two great edifice collapses (Vallance et al. 1995).

Fuego's 1974 activity

The October 1974 eruption deposit (Fig. 1, inset), mapped by Rose et al. (1978), consisted of four water-poor (in terms of eruptive conditions and, essentially, deposition) vulcanian to subplinian explosive events that occurred over a 10-day period, which if taken together represent the largest (about 0.1 km³ DRE) of a series of at least 24 remarkably similar events from 1944 to 1976 (Rose et al. 1973; 1978). From 1976 to 1979 Fuego changed its style of eruption to less explosive and more continuously-active, with the venting of lava flows (Martin and Rose 1981). From 1979 until November 1998 it only emitted gas (Andres et al. 1993). In May 1999, a small basaltic explosion and accompanying lava flow marked an end to this unusually long repose. Since 1999, except for a quiet one year period during 2001, Fuego has been sporadically active with small tephra eruptions and associated lava flows and block-and-ash flows during activity similar in style, intensity, and magnitude to that of the 1976–1979 period. It is notable that the October 1974 activity alone yielded about 10% of the total output of the volcano over the past 450 years.

The 1974 eruption sequence commenced on October 10 following 20 months of relative inactivity. The first subplinian phase occurred on October 14 (see Stoiber (1974) for photographs of the event). Studies of the four 1974 eruptions that occurred from October 14–24, as well as details on the location and setting of Fuego, were summarized by Rose et al. (1978). Between October 14 and October 23, magma composition varied, but only slightly (Fig. 3; see Rose et al. 1978 for stratigraphic compositional details).

Eruption columns reaching the lower stratosphere were generated on October 14, and this event produced the second largest stratospheric injection of the four main explosive phases during the eruption, the major one being on October 17–18. Significant stratospheric aerosol perturbations and possible associated stratospheric temperature decreases were documented for the months after October 1974 (e.g. Volz 1975; Meinel and Meinel 1975; Hoffman and Rosen 1977; McCormick et al. 1978; Lazrus et al. 1979). In other papers, we presented data pertinent to the stratospheric injection of dust and gas from the Fuego eruption (Murrow et al. 1980; Rose et al. 1982). A secondary focus of this study is the fate and transport of fine ash particles (<30 μm in radius), which can have a long atmospheric residence time. Note that the expectation is particles of this size, because of their low settling velocity, would not deposit on-land unless premature removal is

enhanced by aggregation processes. We have included data on fine particles (< 50 μm diameter), which are often ignored in size distribution studies of fall deposits, because these particles cannot be separated by sieves, the usual tool for volcanic tephra sizing studies. This paper is partly motivated because recently there has been a growing awareness that such fine particles are important in hazard assessment because of their impact on aircraft and human and animal health.

Distribution, character, volume, and mass of the October 14, 1974, deposit

The climax of the October 14, 1974, eruption lasted about 5 h, with closely-spaced explosions and a stratospheric, sustained eruption column together with minor collapses which generated pyroclastic flows (see Rose et al. 1978 for eruption details; Davies et al. 1978 for details of the pyroclastic flow deposits). Mapping and collection of freshly-fallen tephra of the 14 October eruption was carried out on 15–16 October by Samuel Bonis of the Instituto Geográfico Nacional, Guatemala City, at distances ranging from 7 to about 80 km from the volcano. This sampling effort

continued throughout the following 10 days and involved the entire October 14–23 eruptive sequence. In all, > 350 well-documented samples of scoriaceous ash and lapilli were collected from the 1974 Fuego eruptions and have provided the basis for more than 40 research papers to date.

Tephra distribution

Each of the four 1974 explosive events occurred while the winds were blowing to the W or WSW (Fig. 4), resulting in simple fallout dispersal patterns (Fig. 1). No tephra fell on the E slopes of Fuego or in the area between Guatemala City and Escuintla. This we suggest was due mainly to the low level inflow of cool air which must have swept up the E flanks to replace the heated air being transported upwards in the vigorously convecting column. Also, wind flow would be expected to accelerate around this large cone and particles falling upwind of the vent would be expected to be re-entrained, as can readily be observed in experiments of sedimenting turbulent plumes in a crossflow (Ernst 1996). Overall, both the October 14 and the whole 1974 tephra blankets are smaller in area than Plinian deposits (Fig. 5), and consistent with subplinian dispersal.

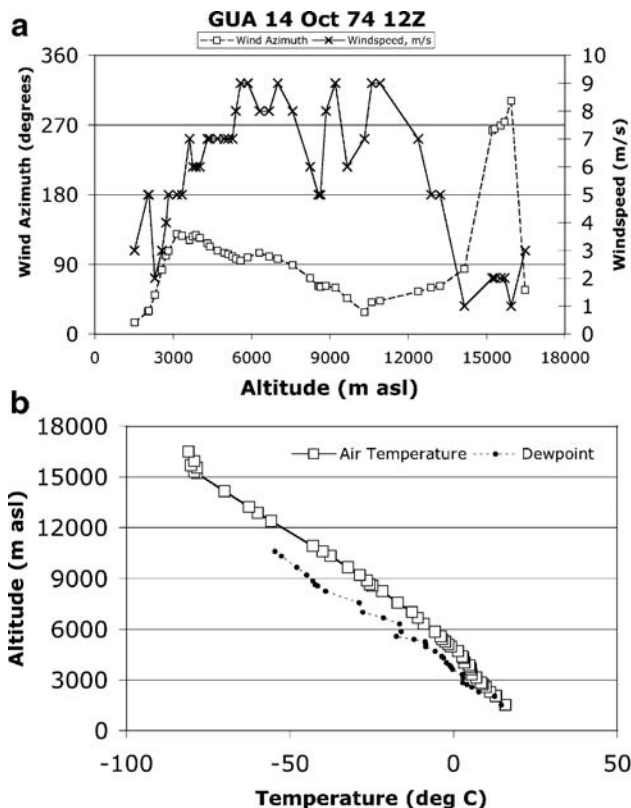
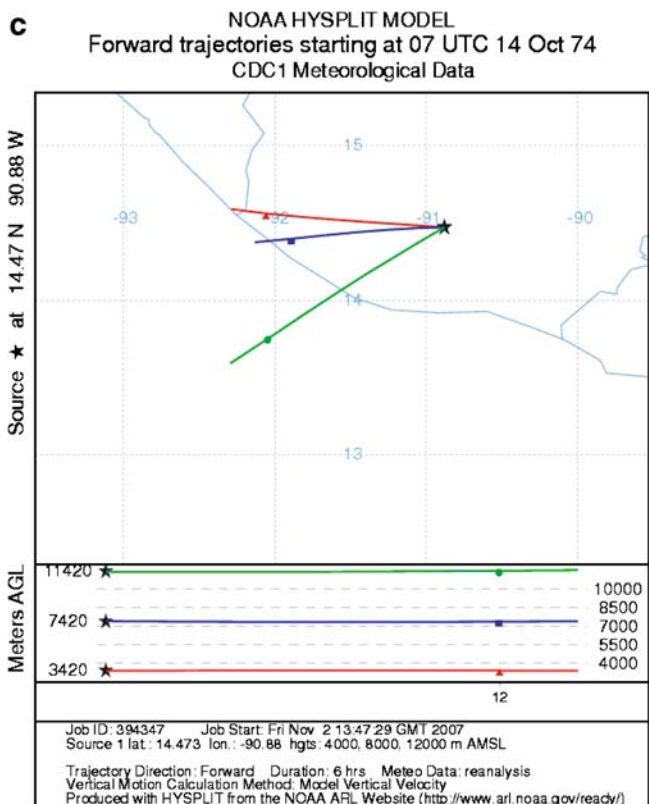


Fig. 4 a,b Radiosonde data from Guatemala City (GUA), 40 km NNE of Fuego Volcano at 1200 UT on 14 October 1974. Above is wind direction and speed, below is temperature and dewpoint. Data from NCDC 1995. **c** HYSPLIT 6-h simulations (Draxler and Hess 1998) of ash eruption of Fuego beginning at 0700 UT, 14 October 1974,



showing the dispersal of ash to the west. Note that altitudes of 7–11 km carry ash to the WSW, where most bimodal ashfall and the main dispersal occurred, and that lower altitudes of ash are dispersed to the WNW where fine ashfalls occurred

Sampling and grain size analysis procedures

The deposit was sampled to its effective limit as a continuous sheet (~1 mm thickness); outside of this area there was only patchy fallout. Samples were collected before they were rained on because we were interested in measuring scavenged aerosols and adsorbed gases (Rose 1977); wet samples were recorded as such. Most of the samples collected were fresh, dry, and undisturbed, and in areas where tephra sedimentation was sparse, the samples were collected using a toothbrush. No particle aggregates were observed during tephra collection.

Forty samples of primary fallout tephra were selected from the October 14 deposits for granulometric analysis (Fig. 6). Laboratory analyses involved sieve analysis by hand to avoid breakage of pyroclasts. The sub-45 μm fraction was analyzed using a Coulter Counter (see Huang et al. 1975, for application to tephra samples) down to 4 μm . (Analyses were obtained data for sizes < 4 μm but these very small amounts are not reported because we consider the accuracy of the data to be poor.) We have also determined laser diffraction size distributions down to 0.2 μm on a few samples to confirm the Coulter Counter data, especially for samples at the periferies of the ashfall blanket. Both the Coulter and laser diffraction determinations measure projected diameters of particles and we assume a density of 2,000 kg m^{-3} to convert them to weight percent and combine them with mass measurements of coarser particles. The density assumption here is consistent with field and laboratory data that show lower densities for the ash in the field and sample bag, and higher densities for the dense rock equivalent of Fuego's high Al basalt (taken here as 2,750 kg m^{-3}). We have no specific data to support our assumption of 2,000 kg m^{-3} , however, the real value should be assumed to be ~ 2,000+700 kg m^{-3} .

Components of the October 14 tephra

The October 14 tephra fall deposit was a single unit (i.e. consistent with a quasy-steady eruption column), not size-graded, and dominantly composed of ash size clasts (< 2 mm). Within 7–10 km of source, scoria lapilli dominate the deposit. The juvenile component is vesicular high-Al basalt (whole rock has 50 wt% SiO_2 ; Fig. 3) consisting of submillimeter-size phenocrysts of plagioclase (An_{95-80}), olivine (Fo_{76-66}), and minor amounts of magnetite, augite, and amphibole in a hypocrySTALLINE groundmass with a SiO_2 content of 52 wt% (Rose et al. 1978). Vesicles and crystals in proximal scoria have a maximum size of approximately 1.5 mm. The sizes and proportions of crystals and vesicles in large scoria lapilli (2–5 cm in diameter) collected near source were determined by point counting in thin sections and are given in Table 1. The scoria lapilli average 38 vol

% vesicles, with a range of 32–47 vol.% (well below the packing limit (Sparks 1978), and significantly less than the 55–75% vesicle content noted by Druitt et al. (2002) for 1997 Montserrat vulcanian fall deposits. Of the solid phases, groundmass and glass account for 62 vol % and 38 vol % is phenocrysts and microphenocrysts (from, rarely, 1.5 mm down to 0.1 mm across). The crystal proportions are most probably representative of the immediate pre-eruptive magmatic proportions because the size of the scoria lapilli (diameters of several cm) is more than an order of magnitude larger than the largest crystals and atmospheric fractionation of crystals and glass could not affect them. The crystal-rich magma was dominantly fragmented to sizes smaller than that of non-groundmass crystals and vesicles (~ 56 wt% of the tephra deposit is ≤ 1 mm, Table 2). We measured the crystal proportions in only eight proximal (7–10 km from source) tephra samples but, from microscopic inspection, the distal tephra fall deposit does not show obvious crystal enrichment over magmatic proportions. Crystal concentration has not been routinely measured (cf. Sparks and Walker 1977) because of the problems of separating such a fine-grained tephra into its constituent components and because of the continuous range of crystal sizes. However, the submillimeter size splits of about 10% of the tephra samples do have proportions of crystals > 50 vol.%. Because of this, we assume that tephra samples with large fractions of submillimeter particles had been subject to atmospheric fractionation. We judge such fractionation to be of secondary importance because Rose et al. (1978) have shown that distal and near source tephra samples of the October 14 activity are nearly chemically identical.

Finer ($\text{Md}_\phi > 4$) tephra samples consist mainly of angular glass pyroclasts, some of which were vesicular and some (especially finer ones with $\text{Md}_\phi > 5$) were non-vesicular (Fig. 7). The shapes of October 14 pyroclasts in the most distal sample of this group (sample no. 200) were characterized by Riley et al. (2003), who showed that clasts of all observed sizes (5–200 μm in diameter) were quite angular overall and had aspect ratios of about 1.5. The terminal settling velocities of pyroclasts were measured and compared with their shape. The long diameters were generally ~ 2 times larger than the diameter of ideal glass spheres with the same terminal velocities.

Due to the sizes and proportions of vesicles, coarser particles generally have a lower density than those too small to include vesicles. In the case of the Fuego tephra fall deposit, particles consisting of free crystals are found generally only in fine size splits ($> 2.5 \phi$). Because coarser particles are larger than the crystals, atmospheric fractionation in the proximal fall areas does not cause crystal enrichment or depletion, and has little effect on the overall

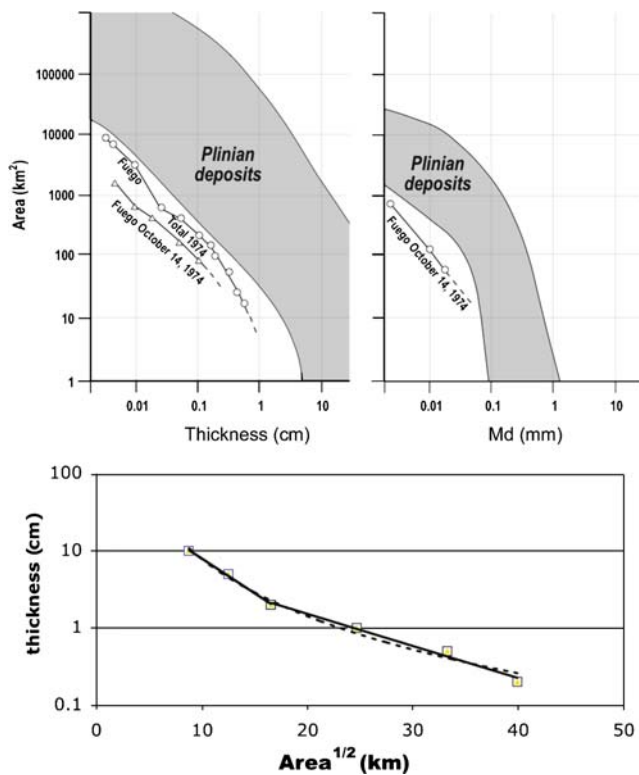


Fig. 5 Top Area (km^2) contained within isopach region plotted against thickness of isopach (m) for the October 14 and total 1974 fall deposits. Stippled field is that of Plinian and ultraplinian deposits (Walker 1982); below Log/log area/thickness plots for the 14 October 1974 fall deposit, using Pyle (1989) method. Breaks in slope (BIS) are indicated (proximal and distal BIS) according to the ideas of Bonadonna et al. (1998) and the T_{max} value intercept (60 cm) is used in Fig. 11. The dashed line shows the powerlaw fit used in the volume calculation (Table 4)

density of the ejecta. Crystals do affect the size distribution of particles in the tephra, however (see below).

There is a significant fraction (up to 10–20 vol.%) of accessory lithic material in the October 14 tephra. This is chiefly oxidized and altered basaltic material, presumably from the walls of the vent and conduit, and possibly includes dense magmatic clasts of residual 1971 magma from the conduit. Lithic material falls out mainly in proximal areas because it is generally not as fine-grained as magmatic pyroclasts (see Rose et al. 1978). The morphology of magmatic grains of the October 14 Fuego tephra are illustrated in SEM views (Fig. 7) of sample 200, distal tephra fall.

Grain size and sorting

The October 14 tephra samples generally fine with distance from the volcano (Fig. 8) and are dominantly well-sorted (Fig. 9), with standard deviation ($\sigma_{\phi} = (\varphi_{84} - \varphi_{16})/2$; Inman 1952) between 0.25 and 1.00. Sorting decreases out to 20 km along the dispersal axis and then remains near-constant, as is the case for many tephra deposits from dry

magmatic eruptions. Sorting improves as the overall grain size decreases if samples far from the dispersal axis are excluded (Fig. 9). Most samples are unimodal (Figs. 10, 11), i.e., they have > 90 wt% of the size distribution within one standard deviation of the mean. In unimodal samples the mean grain sizes are between about -1 and 2φ (2–0.25 mm). Some samples (see Figs. 11 and 12) have a small fraction in the fine mode (10–15 wt% of $\sim 4-6\varphi$ (16–63 μm), with the exception of samples from the periphery of the fallout area which are clearly bimodal (discussed below). Median diameter ($\text{Md}_{\phi} = \varphi_{50}$ (Inman 1952) decreases both downwind and transversely across the dispersal axis (Figs. 11 and 12). The overall spatial pattern is shown in Fig. 13.

Grain-size distributions (GSD) of October 14 tephra are examined on traverses across and along the dispersal axis (Figs. 10 and 1). Across the axis, selected samples show the size distribution at the N edge is bimodal, with modes at 2φ (0.25 mm) and 5φ (0.031 mm). The character changes abruptly away from the northern edge and in the transverse section (Fig. 10). The three samples representing the main part of the dispersal (samples 29, 32 and 48) are essentially unimodal (mode at $1-2\varphi$, 0.25–0.5 mm) with extremely subordinate modes at $4-5\varphi$. This pattern is typical of most samples, both across and along the dispersal axis. At the S edge (sample 52, Fig. 10), there is still a coarse mode at 1φ but the subsidiary, finer mode has become larger. There is a systematic relationship with distance for the coarse mode for samples along or near the dispersal axis (Fig. 13), but a coarser lobe (most obvious in the 1φ isopleth) persists to the S edge of the deposit.

In a downwind traverse (Fig. 11), as near to the dispersal axis as sampling allowed, the data show largely unimodal character, with a persistent though very minor secondary mode at 4φ (samples 80, 20, 71, 35 and 43). The coarse mode fines from -2 to -1φ (2–4 mm) at 8 km from source to -1 to 0φ (1–2 mm) at about 12 km, to $2-3\varphi$ (0.125–0.250 mm) at 55 km. Only at the edge of the recognizable deposit is a considerable fine mode seen; sample 200, collected at 78 km from vent but 24 km N of the dispersal axis (Fig. 6), shows a large (~ 20 wt%) fine mode. Sample 200 (and others in Fig. 12) is bimodal, the prominent coarser mode documented in the other downwind samples is at 4φ (0.063 mm) and has almost merged with the persistent fine mode (5φ) in samples 200 and 252. An even finer mode also occurs (7φ , 0.008 mm) that was not detected in any significant amounts elsewhere in the dispersal area. This must be fine dust that does not occur in the continuous tephra blanket, and we are unsure how to estimate how much of this material was dispersed. We analyzed sample 252 using laser diffraction methods which allowed for a better determination of size modes (Fig. 12). The GSD of sample 200 is broad and fine skewed, and can

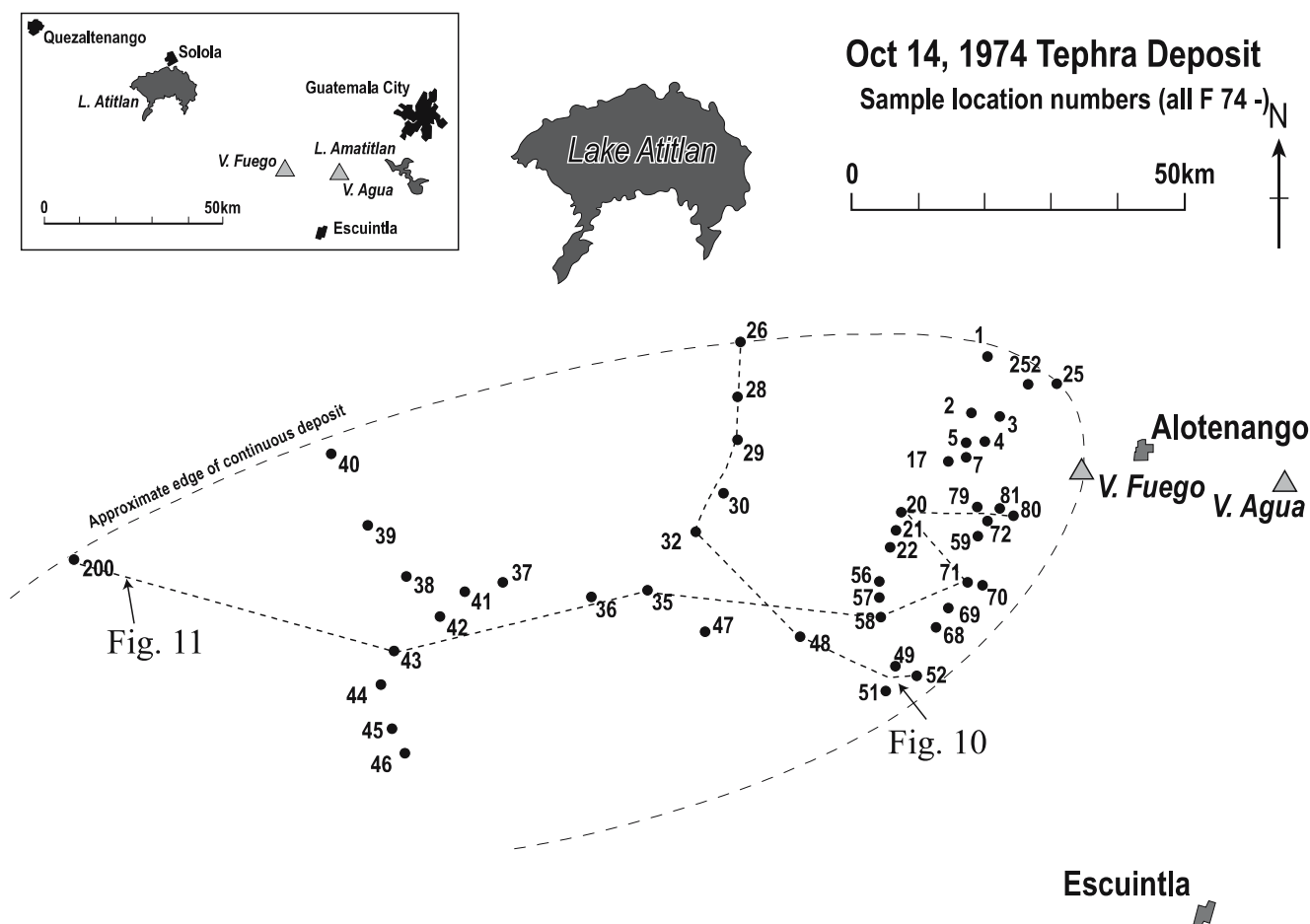


Fig. 6 Map showing locations of individual samples of the October 14 tephra deposit, with sample numbers. Collection sites of samples plotted in Figs. 1, 10, 11, 12 are indicated

best be described as consisting of a coarser mode at $\sim 3.1\phi$ (117 μm) and a finer mode at $\sim 4.9\phi$ (33 μm) (Fig. 12).

Coarse and fine modes in the size distribution

Grain size distributions of October 14 tephra samples are generally unimodal, with a prominent, variable size, coarse mode (-2 to 3ϕ) and a small but persistent fine mode at $\sim 5\phi$ (32 μm) that only becomes prominent on the very edges of the fallout area (Fig. 12). The behavior of the coarse mode, combined with SEM examination of the samples (Fig. 7; see also Rose et al. 1978; Riley et al. 2003), suggest that it results from explosive fragmentation of the vesiculating porphyritic magma with liberation of crystals (average modal size 0.25 mm). The origin of the subordinate fine mode is of particular interest in this case, see later discussion (Figs. 14 and 15).

Overall, the October 14 tephra fall deposits have two populations of particles. The coarser particles consist of vesicular groundmass with contained crystals and have a lower density, whereas the finer particles are glass shards

Table 1 Summary of petrographic characteristics of Fuego October 14, 1974, magma (after Rose et al. 1978, p. 12)

Phase	Modal amount Percent (ave. of 8)	Range Percent	Size (mm)	
			Mean	Range
Crystals > 0.1 mm				
Plagioclase	31	18–51	0.39	0.14–0.81
Olivine	3.6	n.d. ^b	0.47	0.15–0.86
Clinopyroxene	0.8	n.d.	0.35	0.14–0.76
Magnetite	2.6	n.d.	0.23	0.12–0.52
Total:	38.6			
Groundmass ^a and glass	61.4	n.a.	n.a.	
Crystals + groundmass + glass	62			
Vesicles	38	32–47	0.33	0.05–1.30

Determined by point counting of thin sections:

^a groundmass crystals < 0.1 mm

^b n.d. not determined; n. a. not applicable

Table 2 Total grain size distribution for October 14, 1974, Fuego tephra unit modified from Murrow et al. (1980) (No. 1), using the method by Murrow et al. (1980) but also including 10% pyroclastic flows (No. 2) and using the Voronoi method (Bonadonna and Houghton 2005) (No. 3)

ϕ	Mm	No. 1 wt%	No. 2 wt%	No. 3 wt%
-4	16	1.25	1.26	0.00
-3	8	0.85	0.85	0.00
-2	4	4.33	4.36	7.20
-1	2	8.91	8.97	12.43
0	1	20.20	20.32	27.31
1	0.5	26.64	26.80	27.05
2	0.25	20.49	20.62	16.87
3	0.125	6.24	6.28	4.32
4	0.063	3.26	3.28	1.57
5	0.032	3.03	3.06	1.65
6	0.016	2.36	2.37	0.92
7	0.008	1.14	1.15	0.46
8	0.004	0.45	0.45	0.16
9	0.002	0.15	0.15	0.05
10	0.001	0.09	0.09	0.02

and individual particles are thus denser. The dividing line between the coarse population and the denser, finer one comes at about 0.1–0.5 mm ($3-1\phi$), which is the typical size range of many of the crystals and vesicles in the tephra (Table 1).

Deposit density

The bulk density of the freshly fallen October 14 tephra was measured several times in the field, averaging $1,100 \text{ kg m}^{-3}$ [Bonis, S. B., pers comm, 1975], but detailed data are not available, so in order to further constrain deposit densities the volumes of 60 of the larger samples from the compositionally and texturally similar but smaller eruption deposit from 1973 were measured in a graduated cylinder and the samples weighed. All measurements were performed under the same conditions. Results ranged from 460 kg m^{-3} for a scoria lapilli-rich sample collected 7 km from the vent (but away from the dispersal axis), to $1,400 \text{ kg m}^{-3}$ for a much finer-grained sample collected 31 km from the vent on the dispersal axis. Near source samples vary greatly in density, but variation decreased distally to between $1,280$ and $1,100 \text{ kg m}^{-3}$. The average of all the density measurements is $1,140 \text{ kg m}^{-3}$, in good agreement with the abovementioned field estimate. Such values are higher than densities of freshly fallen tephra from more explosive eruptions (e.g. Sama-Wojcicki et al. 1981; Neal et al. 1994). However, these have largely been of more felsic composition and dominantly vitric, whereas, in contrast, the Fuego tephra comprises mafic juvenile clasts

with abundant crystal fragments, lower vesicularity and minor lithics. Fuego deposit densities are comparable to those measured for vulcanian and dome-collapse tephra deposits in Montserrat (Bonadonna et al. 2002). The deposit bulk densities are much lower than typical particle densities, which range from $\sim 1,500$ to $> 2,700 \text{ kg m}^{-3}$.

Volumes erupted on October 14 and in the October eruption

The October 14 tephra deposit (Fig. 1) had a dispersal pattern showing fairly systematic thinning downwind. The deposit volume was estimated using both a graphical stepwise technique (Fig. 5b and Table 3) and integration techniques (Rose et al. 1973; Pyle 1989; Bonadonna and Houghton 2005) (Table 3). The incremental parts (thick-

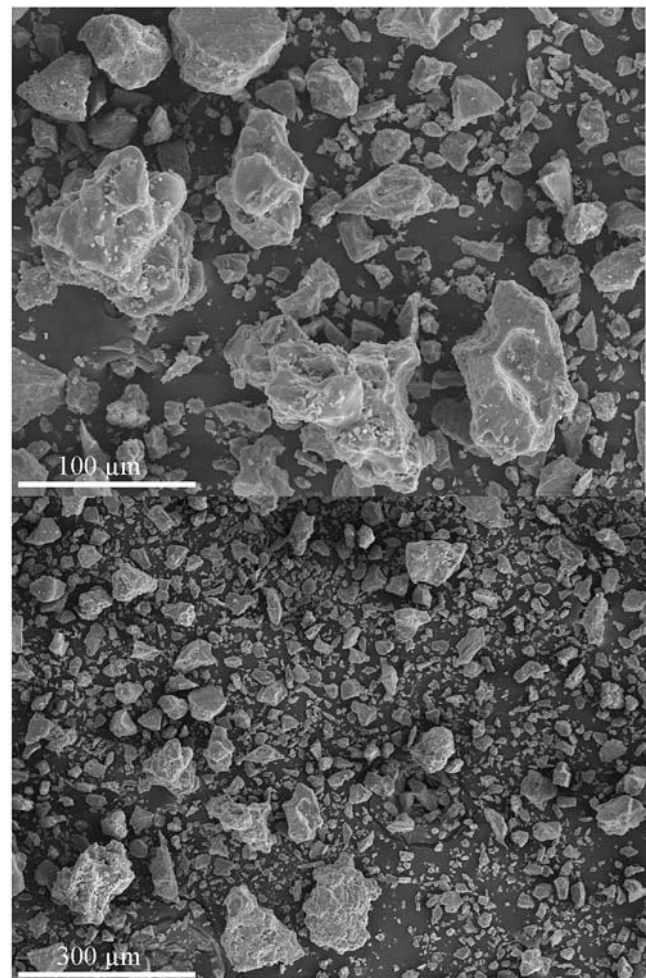
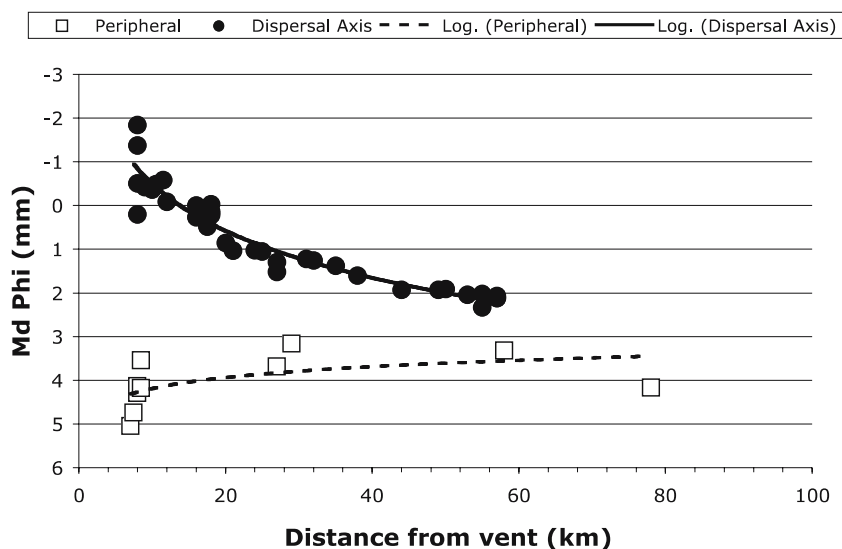


Fig. 7 SEM images of highly angular pyroclasts from sample 200 of October 14, 1974 fallout (see Fig. 6 for location). *Lower view* shows a low magnification view of the whole sample, showing a large variety of sizes. Larger pyroclasts are glassy with included phenocrysts. In *upper view*, at higher magnification, some glassy pyroclasts and some cleavage-bound crystalline fragments can be seen which represent liberated phenocrysts (see text for discussion)

Fig. 8 Median diameter (Md_{ϕ}) for October 14 tephra samples plotted against distance of sample collection site from source. Note that samples collected in the middle of the dispersal region, along and on either side near the dispersal axis, fall on a typical curve, while fine grained, bimodal samples collected at the very northern periphery of the deposit display little change with distance from source

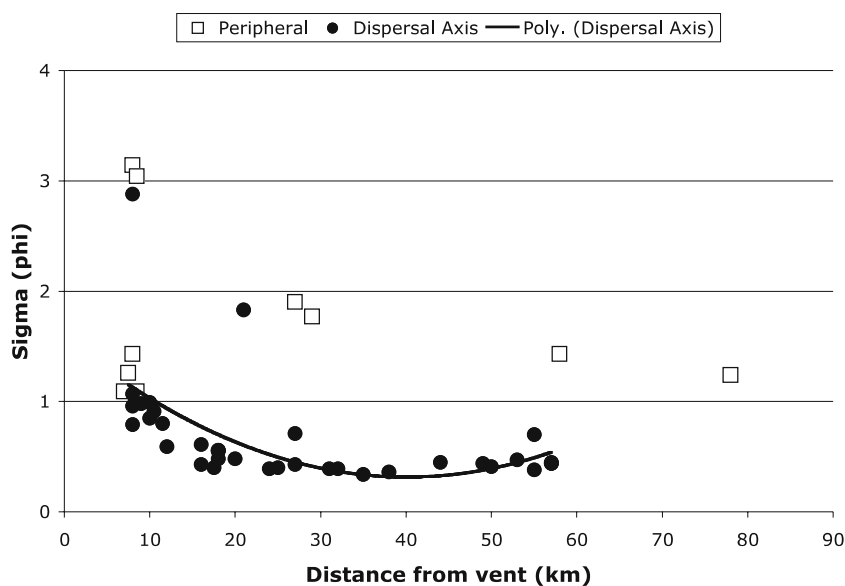


ness, area) of the isopach map can be used to estimate a minimum bulk volume of about 0.036 km^3 (Table 4). Including 10 vol % of pyroclastic flow deposits estimated by Davies et al. (1978; 0.0039 km^3), this gives a minimum total production of 0.039 km^3 on October 14, which converts to a dense rock equivalent (DRE) volume of 0.016 km^3 using $1,140 \text{ kg m}^{-3}$ as the bulk deposit density of $2,750 \text{ kg m}^{-3}$ as the density of dense Fuego basalt (Rose et al. (1978). Plots of area vs. thickness or thickness vs. $\text{area}^{1/2}$ (Figs. 5, 16) allow comparison of the isopach data of the October 14 deposit with others from the literature, and a more holistic estimate of the volume. The thickness vs. area plot is a single linear trend on a log/log scale (Fig. 5a), whereas the thickness vs. $\text{area}^{1/2}$ plot shows a break in slope

at about 16 km (Fig. 5b). Bonadonna et al. (1998) have shown that breaks in slope in thinning trends reflect the transition between different fallout regimes (i.e. fallout from plume margins/umbrella cloud; turbulent/intermediate regime and intermediate/laminar regime of fallout from the umbrella cloud).

By analogy with other eruptions it is very difficult to know how much volume of tephra was carried beyond the last measured isopach, and how much larger the total volume erupted may be. A maximum of 15 wt% was indicated by Murrow et al. (1980) from the Rosin/Rammler analogy for the overall size distribution. This “missing” fine ash was widely dispersed beyond the perimeter of recognizable tephra deposit. Application of the Pyle method to the plot

Fig. 9 Plot of σ_{ϕ} (sorting) vs. distance from vent for samples of October 14 tephra. Samples near the dispersal axis are better sorted than peripheral samples, and become better sorted with distance, especially between 10 and 20 km distance



shown in Fig. 5b, and including 10% pyroclastic flow deposit volume gives total volumes of 0.041 km^3 , which converts to a DRE volume of 0.017 km^3 . Use of a power law volume calculation for the fall deposit (Bonadonna and Houghton 2005), which implicitly means that the most distal ash to fall out would have escaped premature fall induced by aggregation, yields a volume of 0.046 km^3 (Table 4). Including 10% pyroclastic flow volume to the tephra deposit yields a total volume of 0.051 km^3 and a DRE volume of 0.021 km^3 (or $5.8 \times 10^{10} \text{ kg}$).

Comparison of this integrated volume, which extrapolates to both maximum and minimum thicknesses beyond the range of isopachs, is higher than the simple sum of isopach-contained areas and shows that up to one third of the total fallout mass could be fine ash that fell outside of the last measured isopach, providing ash aggregation did not occur. The range of such estimates, from 6 to 33% is speculative and representative of our lack of truly constraining data. The uncertainty about fine ($>4\phi$) ash occurs because the distribution of fines is irregular and cannot be generalized and mathematically extrapolated from the pattern of GSD in fallout samples in the same way that coarse pyroclast sizes can. In recent studies using data from satellite-borne instruments [e.g., Wen and Rose 1994; Krotkov et al. 1998] estimates of only a few % of fine ash are indicated for drifting volcanic clouds [see also discussion by Bonadonna et al. 1998]. However, a large proportion of fines forming larger aggregates would be invisible to the satellite sensors used, so the minimum missing volume based on Pyle's method may be a better estimate than satellite-derived ones (Schneider et al. 1999).

The bulk minimum volume of the total October 1974 tephra deposit within the 0.2 cm isopach was slightly more than 0.2 km^3 , equivalent to 0.08 km^3 DRE volume of magma erupted (Rose et al. 1978), or $2.2 \times 10^{11} \text{ kg}$. This is about 4 times the volume of the October 14 event alone (see also Rose et al. 1978). Another 0.01 km^3 DRE was estimated for pyroclastic flow deposits which were observed to travel down the cone in all four major pulses during 1974 (Stoiber 1974; Davies et al. 1978). On a plot of area vs. thickness (Fig. 5b) there are several inflections in the curve, probably reflecting that the total 1974 deposit is composed of superimposed fall units, each with a slightly different dispersal area or possibly superimposed co-ignimbrite contributions. Dispersal of tephra over the Pacific Ocean (outside of the area on the inset map in Fig. 1) were estimated by extrapolation of the area vs thickness curve. Extrapolating tephra thicknesses to the trace isopach could increase the bulk volume for the total October 1974 deposit to 0.4 km^3 (or $\sim 0.16 \text{ km}^3$ DRE), but these extrapolations are poorly constrained, as Bonadonna et al. (1998) have shown.

Total grain size distribution of the October 14 pyroclastic deposits

Initial populations of clast size are important when considering eruptive mechanisms such as magma fragmen-

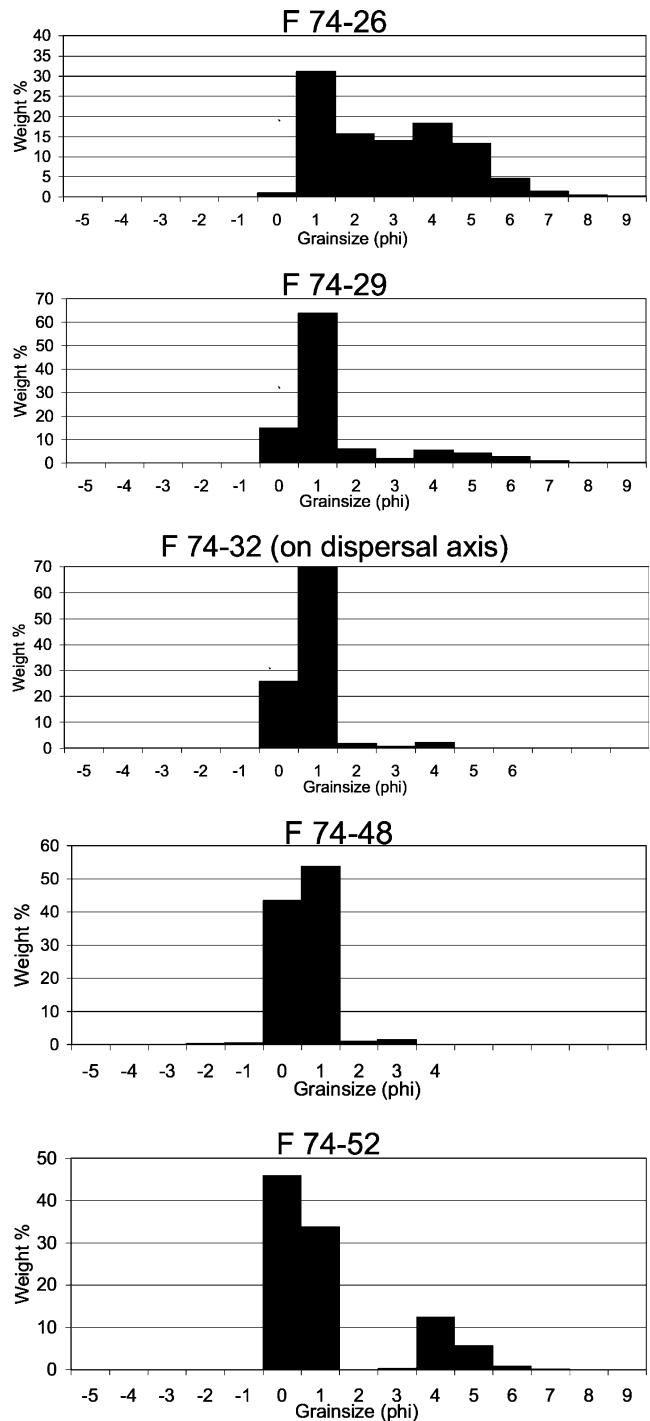
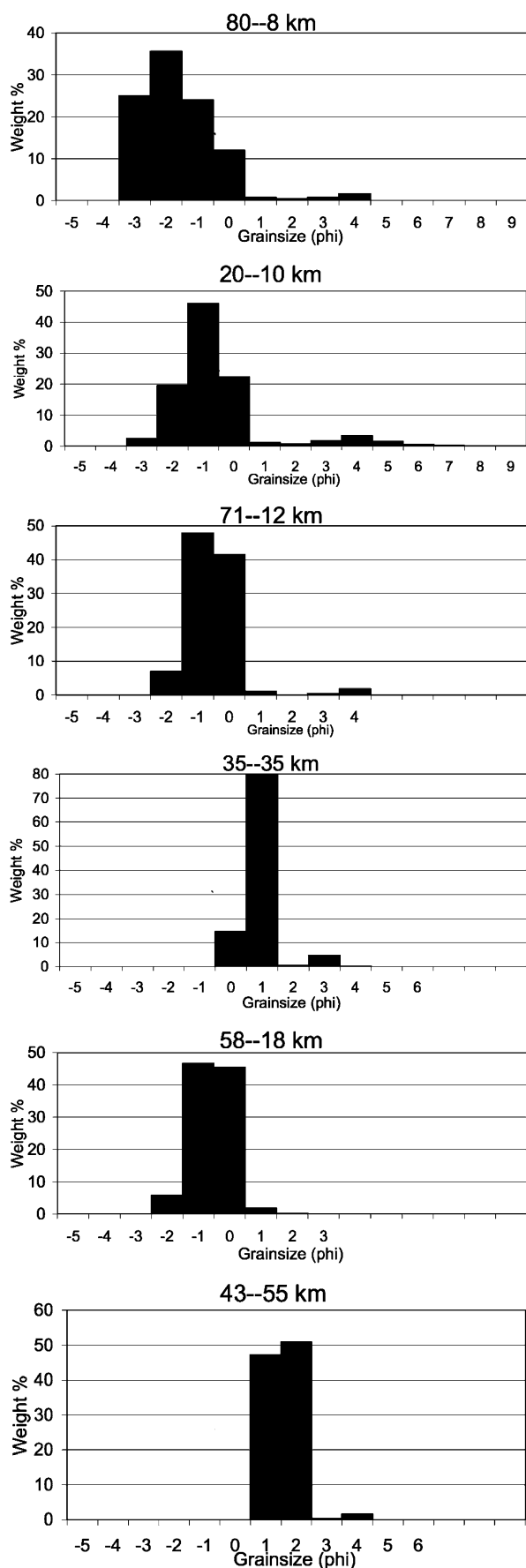


Fig. 10 Frequency curves of five samples representing a traverse from NW-SE across the dispersal axis at a distance of approximately 23 km downwind from vent. Sample 32 is from the dispersal axis of the deposit. Locations of these samples are shown in Fig. 6



◀ **Fig. 11** Frequency curves of five samples collected along or near the dispersal axis at varying distances downwind from Fuego. Locations of these samples are shown in Fig. 6

tation and particle heat transfer rates in the eruption column (e.g. Sparks et al. 1997). Knowledge of the grain size distribution erupted during explosive eruptions is also indispensable for simulating volcanic hazards from ejecta fallout or pyroclastic flows. Fine particle masses must also be estimated to assess health and aircraft hazards. An estimate of the total grain size distribution (initial population) of the Fuego October 14, 1974 ejecta was previously presented by Murrow et al. (1980). Here we report the same data, with slight modifications (Table 3), in order to compare it with other more recent estimates of total grain size distributions of other tephra deposits. Modifications relate to a more accurate estimation of volume increments for the isomass map (Table 3).

The whole-deposit (flow + fall) grain size distribution (Fig. 13 and Table 2) was estimated by Murrow et al. (1980) from the average in each isopach interval, and in the flow deposit, weighted according to the minimum volume contribution of each to the total volume of deposits. We have recalculated this using slightly corrected data for sample positions (Table 3). Although poorly sorted and generally coarser than the fall deposits, pyroclastic flow deposits are typically fines-depleted due to elutriation during flowage and development of co-pyroclastic flow (or co-ignimbrite) plumes (Walker 1981b). Given that some of the co-PF ash is typically sedimented in very distal areas and often out to sea, the total grain size distributions may be fines-depleted. The estimated whole-deposit distribution is unimodal, with $Md\phi=0.58$, $\sigma_{\phi}=1.53$ and $\alpha_{\phi}=0.57$. We also used the Voronoi method to estimate the total GSD of the tephra deposit (Bonadonna and Houghton 2005) and compare the different results in Table 4. The Voronoi method ($Md\phi=0.05$, $\sigma_{\phi}=1.4$ and $\alpha_{\phi}=0.04$) gives a slightly coarser (by $\sim 1\phi$) and virtually zero-skewed (i.e., near symmetrical) distribution (Fig. 16). These total GSDs may be approximated by one dominant mode ($0.1\text{--}0.5\phi$; $07\text{--}09$ mm; $84\text{--}93\%$ of total mass) and two minor modes at -2.48 to -2.25ϕ ; $48\text{--}56$ mm and $4.75\text{--}4.86\phi$; $34\text{--}37\mu\text{m}$. The 5 mm modes comes from the coarse materials in (s and only represents a few % of the total mass. The $35\mu\text{m}$ mode may reflect milling in the pyroclastic flows and elutriation and it amounts to $4\text{--}9\%$ of the total mass (Fig. 16).

We feel that these computed size distributions are valid estimates of the initial population for this short eruptive episode, with the exception of the “missing” volume of fine material (Murrow et al. 1980, and above), which will tend to make the size distribution finer overall, and perhaps less positively-skewed. Walker (1980, 1981a) used a method based upon the mass of each size class to

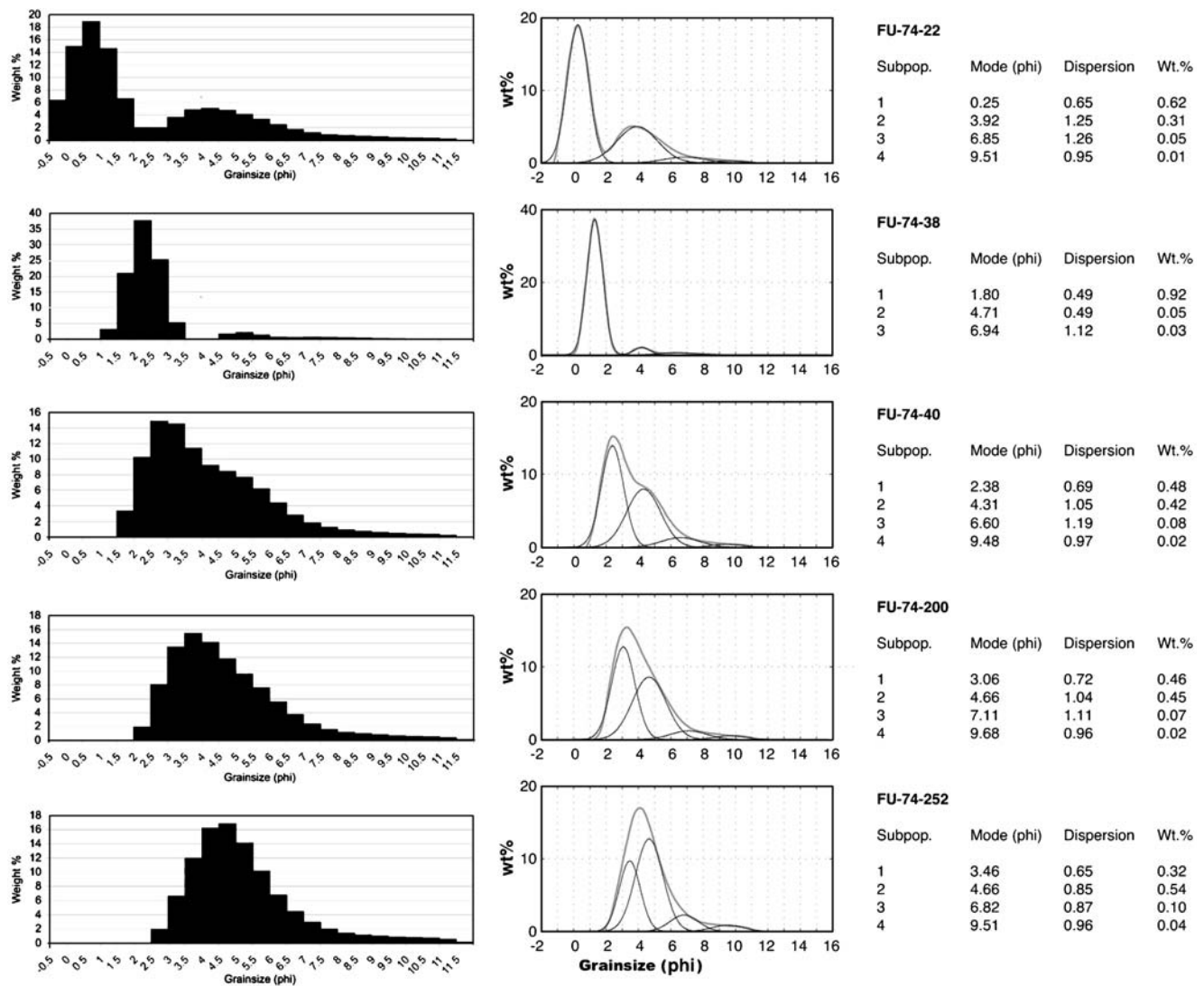


Fig. 12 Frequency curves of laser diffraction GSD for five samples along the north edge of the fall deposit (see Fig. 6 for location of the samples). Note the bimodal character of some samples (22 and 38) and the unsorted finely skewed nature of others (200, 252). To the right of each histogram is a smoothed curve of the GSD and lognormal deconvolutions showing individual modes using the SFT

program of Wohletz et al. (1989). Note that a persistent mode of about 4.5ϕ occurs in all samples while a coarser mode is variable in both median size and proportion in these samples. In two of the samples shown here (200 and 252) the two modes overlap, making for a fine skewed, unsorted GSD

estimate the total grain size distribution of tephra deposit in the Taupo and Waimihia ultraplinian deposits, and showed that these comparatively dry Plinian events have more fine-skewed initial populations than the Fuego tephra deposit. However, a significant proportion of these deposits fell out at sea, so no detail of the size distribution in the sub- 2ϕ classes could be determined. The Hatepe and Rotongaio phreatoplinian tephra deposits (Walker 1981b) retain much more of their initial population character due to their “wet” eruptive and depositional conditions, due to rain washing, particle aggregation, and possibly other mechanisms that promote premature flushing of fines from the eruption cloud (e.g. ice overgrowth on particles—Rose et al. 1995; Textor et al. 2006a,b).

Walker (1981b) commented on the similarity of the high amount of fines in these deposits to that determined for the Taupo and Waimihia Plinian deposits (all four of them had $> 68 \text{ wt\%}$, finer than $< 2 \phi$ (0.25 mm), cf. 17 wt% for the Fuego tephra). Perhaps the most complete total grain size distributions available for felsic tephra deposits come from the 1980 Mount St. Helens (MSH) Plinian eruption and the Ruapehu 1996 subplinian eruption (Bonadonna and Houghton 2005). The high quality of the data is due to the rapidity with which samples were collected and the good coverage of the dispersal area. For the MSH eruption, a strongly fine-skewed grain size distribution was determined by Carey and Sigurdsson (1982) by averaging grain size distributions across the dispersal axis within sub-

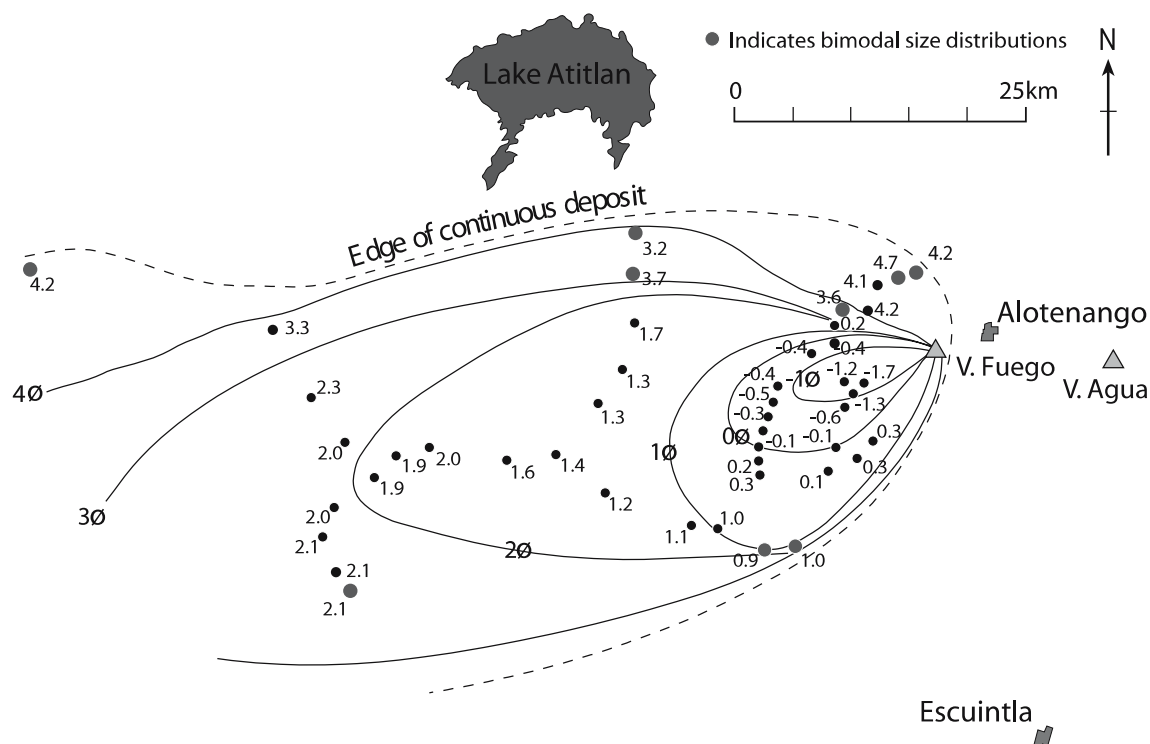
Md ϕ Oct 14, 1974 Tephra Deposit

Fig. 13 Map showing the distribution of Md_ϕ values of samples of the October 14 fall unit. Note the slightly coarser lobe to S (1ϕ isopleth), and very fine, generally bimodal, samples on edge of

deposit. Grey sampling points indicate a bimodal grain size for that sample, while black dots represent samples that are unimodal

rectangular areas containing known proportions of the total mass of the deposit. For the Ruapehu eruption a unimodal, coarse-skewed grainsize distribution ($\alpha_\phi = -0.01$) was determined applying the Voronoi Tessellation method (Bonnadonna and Houghton 2005). The resulting median diameter and sorting are respectively coarser ($Md_\phi = -0.8$) and larger ($\sigma_\phi = 2.4$) than those determined here for the Fuego tephra fall. The Ruapehu eruption was characterized by bent-over plumes and did not produce pyroclastic flows.

The estimated initial grain size distributions for the Fuego and Ruapehu tephra deposits, are much coarser and zero-skewed to perhaps slightly positively skewed, as opposed to negative skewness in most other initial populations (Fig. 16). Part of this difference could be explained by the missing population of fine ash (see above). In contrast to Fuego, the Ruapehu tephra deposit was not associated with co-PF plumes. The coarser grainsize of the Fuego and Ruapehu tephra fall deposits thus appear to be a fundamental characteristic of subplinian eruptions as opposed to more powerful Plinian eruptions. The Fuego initial GSD population is unimodal at both 1ϕ and 0.5ϕ intervals (Rose et al. 1983, their Fig. 3), and is also unimodal without incorporation of the pyroclastic flow deposit data (Fig. 16). Unimodal size

distributions were earlier proposed for other vulcanian/subplinian deposits from Fuego and Cerro Negro volcanoes, although based on fewer data points (Rose et al. 1973). In contrast, total grainsize distributions of Vulcanian explosions from the Soufrière Hills Volcano, Montserrat, are typically bimodal, showing a larger sorting and a larger median diameter than Fuego tephra (i.e. $2.0 < \sigma_\phi < 2.9$ and $3.7 < Md_\phi < 4.6$). However, the two populations shown by the collected Montserrat samples vary between $4.5 < \phi < 5.2$ and $0.2 < \phi < 1.7$ respectively. As a result, the mode of the coarsest population of Montserrat tephra is in the range of the Md_ϕ determined for Fuego (i.e. -1.7 to 1.7ϕ). This was explained with the fact that the Montserrat tephra deposits had a larger contribution from the co-PF ash and therefore was richer in fines. In fact, the fine population of the Montserrat tephra was interpreted as mainly particles from co-ignimbrite ash plumes (Bonnadonna et al. 2002).

Eruption column height and tephra dispersal on October 14, 1974

In the October 14 event, 0.021 km^3 (DRE) of material was erupted in a minimum of about 5 h, assuming that the bulk of the ejecta was emitted during the climactic part of the eruption. This gives a maximum volume flux of erupted

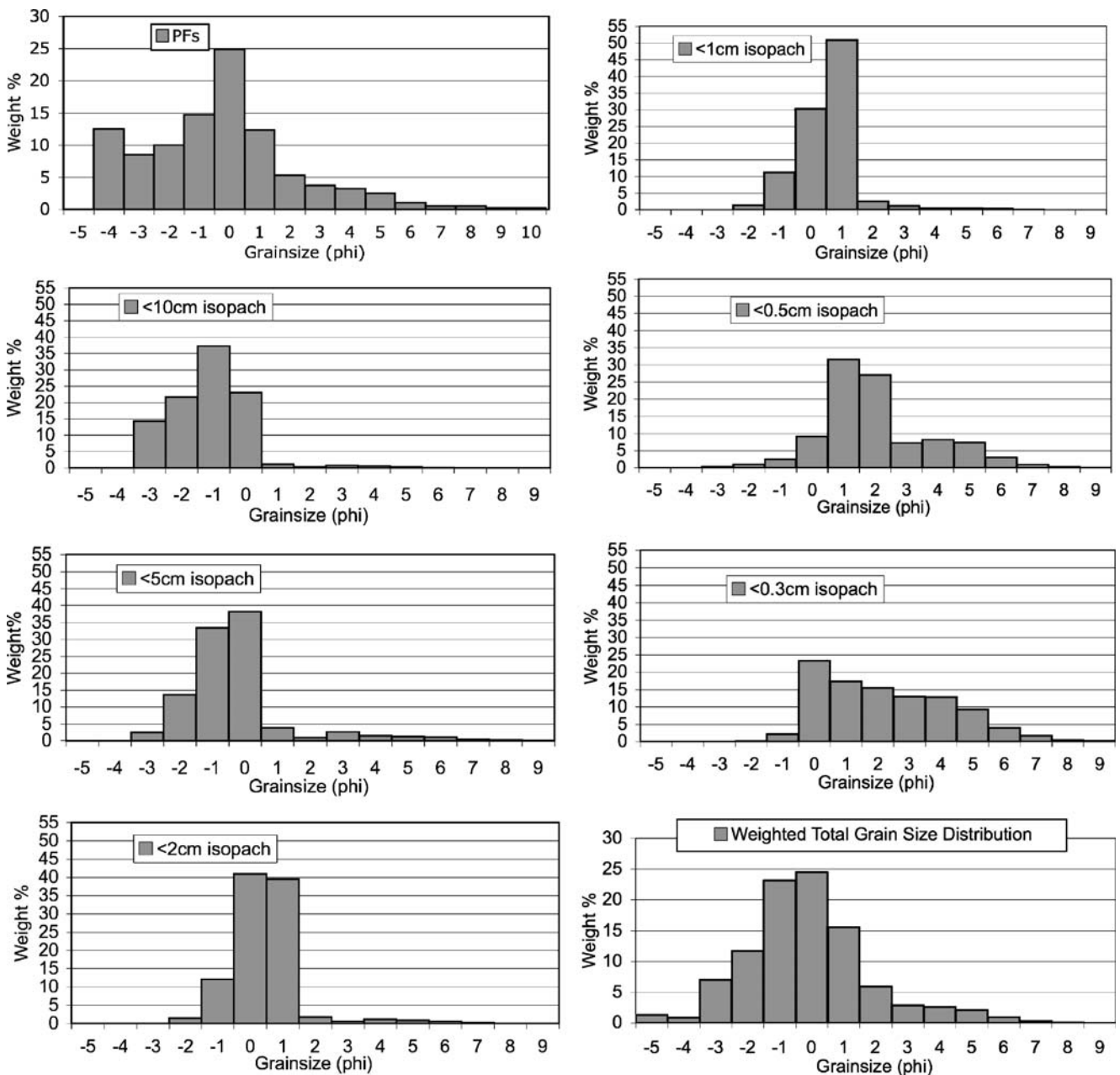


Fig. 14 Average grain size distributions shown as frequency plots for isopach intervals as on Fig. 1 (top) and for the pyroclastic flows. Bottom: total grain size distribution of Fuego October 1974 pyroclastic

deposits (top left) and other deposits, after Murrow et al (1980). See Table 3 and text for discussion and then see Fig. 16 and Table 2

material (not all of it fresh magma) of $1.1 \times 10^3 \text{ m}^3 \text{ s}^{-1}$, equivalent to $3 \times 10^6 \text{ kg/s}$. According to recalculations of plume heights based upon thermal output (Sparks et al. 1997, pp 118–119), a convective column height slightly greater than 10 km above the volcano is suggested by this mass eruption rate. The total column height above sea level (asl) would therefore be $\sim 14 \text{ km}$ for the October 14 eruption, consistent with stratospheric injection for this eruption (the summit elevation of Fuego is 3.7 km). This height compares with an estimate of 17 km asl that can be

made from the position of the distal break in slope in Fig. 5 b, based on Bonadonna et al. (1998).

Radiosonde data from Guatemala City on 14 October 1974 shows E-ESE winds of 3–9 m/s from 2.5–7.5 km asl and ENE to NNE winds of 5–9 m/s from 7.5–15 km asl (Fig. 4). The tropopause was at about 14 km, and the temperatures at the tropopause were $< -75 \text{ C}$, or in the range for which ice would be expected to form. Dispersal of tephra from the eruption column took place by ENE winds above 7.5 km, probably at a maximum between elevations

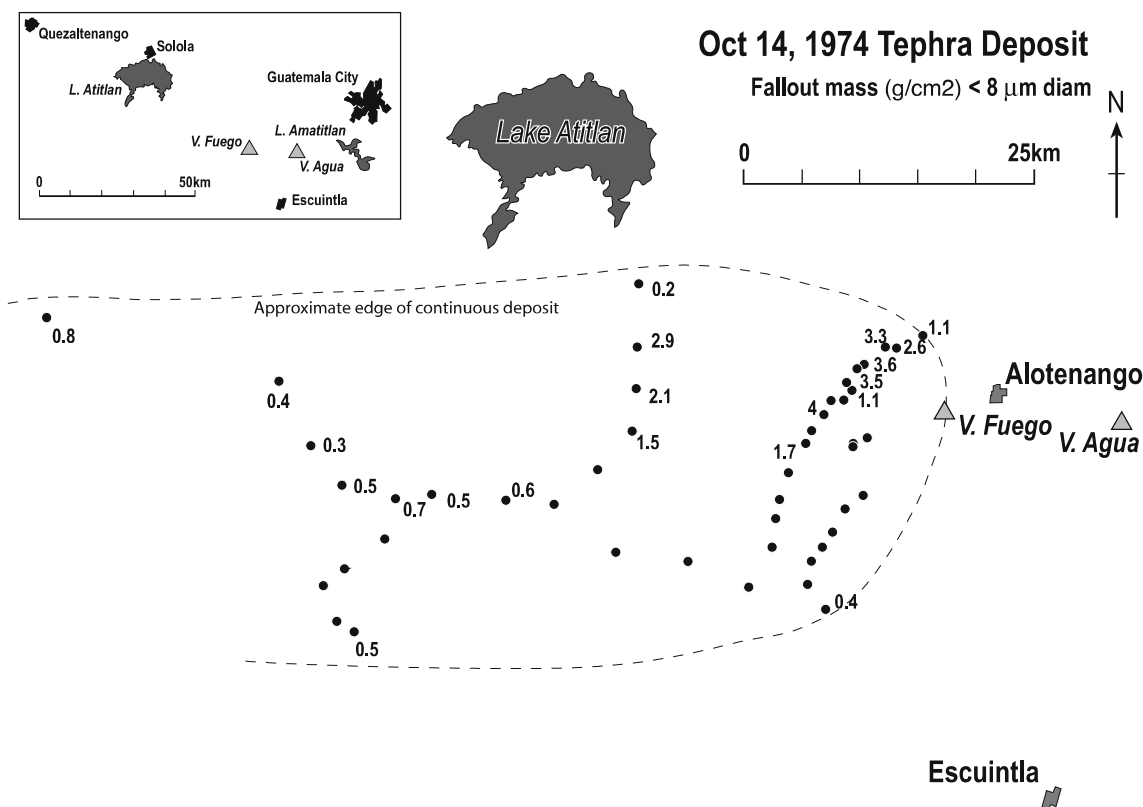


Fig. 15 Map showing masses per unit area in g/m^2 of fine ash (diameter $< 8 \mu\text{m}$ portion of samples plotted in Fig. 6) from 14 October 1974 Fuego eruption. Sample locations which are unlabeled

had mass amounts $< 0.1 \text{ g/m}^2$. Note high masses along the northern fringe of whole deposit

of about 13 km asl and the top of the cloud at $\sim 15 \text{ km asl}$. A height of 13 km asl was reported for this eruption cloud from ground observations, which was probably the elevation of the base of the spreading cloud. HYSPLIT simulations (Draxler and Hess 1998) (Fig. 4b) suggest ash dispersal by winds at 9–13 km asl can account for the fall deposit.

Several details of tephra transport and deposition can be interpreted from our data. The distribution of the coarsest particles (represented by -5ϕ , Fig. 16) allows crude

estimations of eruption cloud height and wind speed using the method of Carey and Sparks (1986). The column did not spread upwind, so that conditions for applying the method were not optimal; nonetheless dispersal of particles (average particle density 2.0 g/cm^3) at an average height of 13–15 km above the fallout surface are indicated, in reasonable agreement with observations. A crosswind velocity of 12–15 m/s is suggested, although the radiosonde values are lower than 10 m/s and the model of Carey and

Table 3 Incremental bulk volume calculation of the 14 October 1974, Fuego volcano fall deposit

Isopach (cm)	Area (km^2)	Volume (km^3)	Percent of total
10	77	0.0077	19.4
5	157	0.0078	19.7
2	274	0.0055	13.9
1	610	0.0061	15.4
0.5	1,108	0.0055	13.9
0.2	1,594	0.0032	8.1
PF ^a	–	0.0040	10.0
Total	–	0.0397	100.0

^a PF = block and ash flow

Table 4 Volume estimates, Fuego eruption of October 14, 1974

Method	Volume, km^3 ^a	Vol + 10% PF ^a	Reference
Incremental	0.036	0.039	Table 1
Exponential	0.037	0.041	Pyle (1989)
Power Law ^b	0.046	0.051	Bonadonna and Houghton (2005)

^a These volumes can be converted to a dense rock equivalent volume (DRE) by using the measured density of Fuego tephra fall ($1,140 \text{ kg/m}^3$) and the dense rock density of Fuego basalt ($2,750 \text{ kg/m}^3$). Using this correction the DRE volume is $\sim 0.02 \text{ km}^3$

^b for the Power-Law calculation the integration limits considered are 0 and 1,000 km. Halving and doubling the distal limit only changes the volume by 3 and 2% respectively

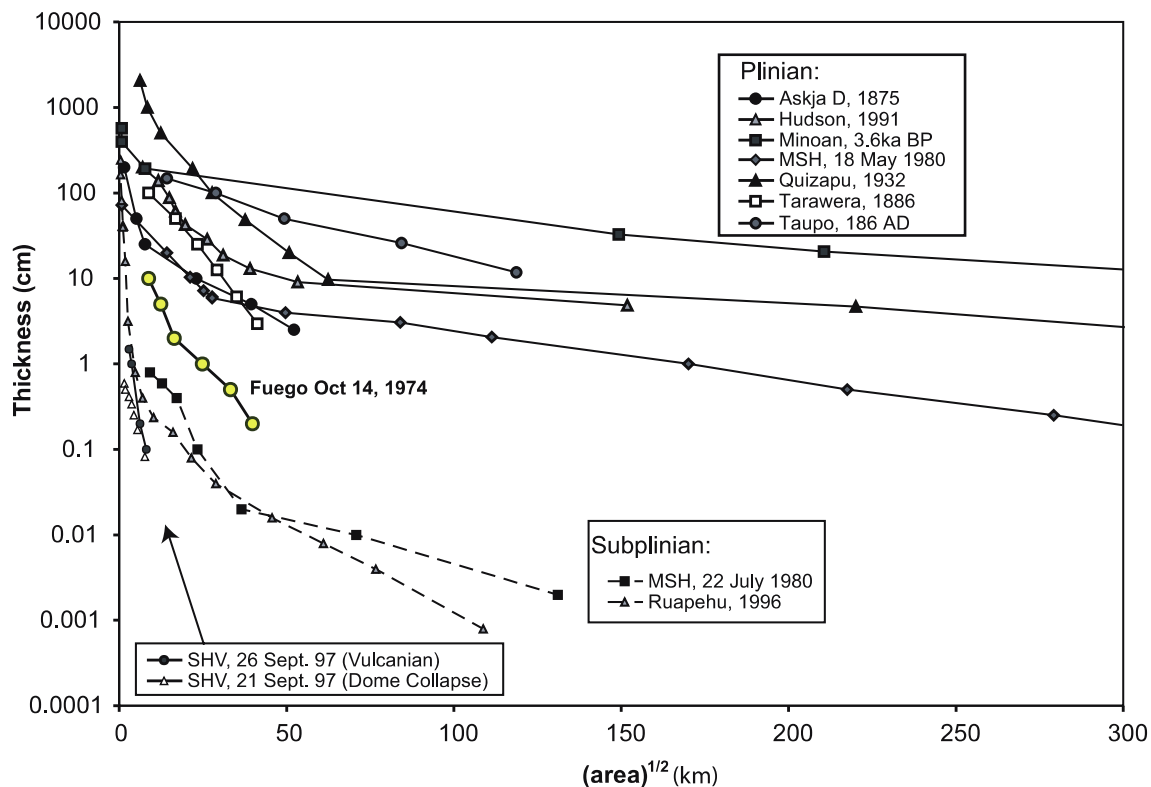


Fig. 16 Semi-log plot of thickness vs. $(\text{area})^{1/2}$ showing the thinning trend of tephra deposits produced by eruptions with different styles and magnitudes (i.e., Plinian, subplinian, vulcanian explosion and dome collapse). Note how Fuego's October 14, 1974, deposit plots between the Plinian and subplinian deposits. References: Askja D,

Sparks et al. (1981); Hudson, Scasso et al. (1994); Minoan eruption, Pyle (1990); Mount St. Helens (MSH), Sarna-Wojcicki et al. (1981); Quizapu, Hildreth & Drake (1992); Ruapehu, Bonadonna and Houghton (2005); Soufriere Hills Volcano (SHV): Bonadonna et al. (2002); Tarawera, Walker et al. (1984); Taupo, Walker (1980)

Sparks (1986) assumes maximum wind velocities at 11 km. Fall times from 18 km asl for particles of various sizes and densities, calculated from the work of Wilson and Huang (1979) and Brazier et al. (1982) range from < 30 min for particles > 1 mm in diameter to > 3 h for particles < 100 μm in diameter. For simple trajectories in a 10 m/s crosswind, it will take ash particles (average density 2.0 g/cm^3) of 100 μm only 3 h to be transported 70 km, i.e. to the edge of the dispersal area. Depending on the extent of aggregation, finer particles may also have fallen beyond. As explained above, we really do not know how much ash was carried farther away, but the tephra blanket ended rather sharply suggesting fine ash aggregation was an effective process leading to premature on-land deposition. Wind velocity was lower than 10 m/s according to the radiosonde (Fig. 4) below 12 km, perhaps as little as 5 m/s, and this slowed the lateral transport of tephra that was drifting at lower levels. A non-trivial factor at Fuego is the almost 2 km elevation difference between the highest tephra sample sites near the foot of Fuego, 1.7 km below the summit, and the lowest tephra sample sites at > 70 km distance and near sea level on the coastal plain of

Guatemala. This selectively adds ~ 2 km to the fall height for distal tephra sampling points.

Fallout of fine mode

The finer fallout mode (< 50 μm in diameter or > 4.3 φ) is prominent especially to the NW (upwind) and at the N edge of the dispersal pattern (Fig. 12). The finest (< 8 μm in diameter) ash must have a very complex fallout pattern and could extend much farther from the vent than is indicated in Fig. 15, perhaps out over the ocean (50 km or more beyond the present extent) in this case. We note that a particle with a diameter of 50 μm would fall to the ground as a single particle after about 12 hours, about 20 times longer than a 1 mm particle (Schneider et al. 1999). The conditions reported from radiosonde (above) reflect relatively weak winds, some wind shear, and with temperatures < -55 $^{\circ}\text{C}$, they were favorable for ice formation on tephra particles and for plume bifurcation, according to Ernst et al. (1994) and Rose et al. (1995). Overall the Fuego plume was a moderately strong one, rising in weak winds and interacting strongly with the tropopause, all factors expected to favor

bifurcation. It is possible that the fines at Fuego were generated from co-pyroclastic flow (co-PF) elutriation, as was suggested for Soufriere Hills by Bonadonna et al. 2002. It also seems likely that microphysical processes (Rose et al. 1995; Herzog et al. 1998; Textor et al. 2005) that could generate latent heat and vorticity and enhance fallout would be more effective in a region where fine particles were more abundant. The more NW distribution of fine fallout suggests that the finer (co-PF?) particles were dispersed by lower level winds at 4–7 km (90–120 azimuth, Fig. 4c) while the main tephra fall was dispersed by winds at 9–14 km (70–90 azimuth, Fig. 4c). It is possible that large particles captured/accumulated fine particles, especially at the edges of the plume (deposit), which explains the presence of coarse and fine modes in those samples (see samples 26 and 52, Figs. 6 and 10). The lower atmospheric air, where the fine (possibly co-PF) ash would be found, is more moist which would aid in fine particle accumulation on coarser more rapidly falling pyroclasts. Rose et al. (2001) describe stage 2 fallout, which takes place mostly from 1–12 hours after eruption and which is associated with fallout of particles too aerodynamically fine to fall as simple particles. In the case of the 1992 eruptions of Crater Peak (Mt. Spurr), this stage 2 fallout formed a secondary maximum of thickness downwind. We speculate that long range transport of fine ash was possibly limited in the case of the October 14 ash plume by its lower transport altitude, with higher moisture potentially enhancing the aggregation and accumulation of fine pyroclasts, and premature fallout.

The pattern of fallout along the N edge of the whole blanket (Fig. 15) may be misleading as an analogous southern-edge, fines-enriched border to the deposit could have been under-sampled in the field effort, although there are signs that it does exist in some southern edge samples (52, 46). Overall, recognition of such a border of fines concentration is new, and differs from the preferential fallout of fines in the “secondary maximum” of thickness in the 1992 Crater Peak (Spurr) deposits (e.g. Rose et al. 2001-See also Discussion section hereafter). This could be a result of a dominant dispersal of co-ignimbrite ash towards the NW due to the prevalent SE character of the low-level winds (Fig. 4). The location of fallout of particles with diameters finer than 10 μm is of interest when considering the health aspects of fine ash, and the result suggests that locations near the edges of potential future tephra blankets should be evaluated for fine-particle health hazards. The presence of a tephra fall deposit with fines enriched along the southern edge of the deposit could reflect co-PF dispersal from a barranca on Fuego’s south flank, because block and ash flows descended on three sides of the cone in the October 14 event.

Discussion

Fragmentation of magma

What process accounts for the fine ash in the Fuego tephra deposit? Can the mechanism of fragmentation be inferred from the characteristics of the fallout materials? Can study of the characteristics of the Fuego tephra blanket teach us about vulcanian/subplinian activity as a whole? We consider that there are several mechanisms that could have formed the pyroclasts: 1. Vesicle bursting, the result of gas escape, an event that is often triggered by shearing or shock wave propagation within an overpressured and stiffened magma (Gardner et al. 1996; Sparks et al. 1997); 2. Breakage of glass at crystal faces; 3. Crystal breakage, possibly driven by melt inclusions; 4. Hydrofracturing from groundwater infiltration; 5. Milling in the vent due to pulsating explosions; and 6. Fracturing, abrasion and milling within pyroclastic flows and subsequent elutriation of fines to the eruption column. Each of these mechanisms has its own set of controlling variables. It may be that tephra deposits with bimodal or multimodal size distributions reflect multiple fragmentation mechanisms.

Vesicle bursting is influenced by the viscosity of the melt, the amount of dissolved gases, pressure gradients, and the degree of shearing or shocking of the magma. It occurs in andesitic magmas such as Soufriere Hills, Montserrat, when a high degree of microlite crystallization increases effective viscosity while the diminishing proportion of magmatic liquid remains volatile-rich (Sparks 1997). Fuego’s magma is more mafic than Montserrat, but still shows a hypocrySTALLINE groundmass likely reflecting solidification within the conduit immediately before or during eruption. Gas loss from the top of the magma column results in undercooling and the partial crystallization of the groundmass. This creates a stiffened cap on the column with high individual overpressures in vesicles, ready for disaggregation by shock waves. We assert that it is likely the most important mechanism, and that the primary (coarser) mode in the size distribution is probably the result of bubble growth/coalescence/bursting dynamics for a gas-rich high Al basalt. We note that the range of observed vesicle sizes (0.05–1.3 mm; mean 0.33 mm; Table 1) is as broad as about 4 φ units (0 4 φ) while 75% of the total grain size distribution also spans 4 φ units (–1 to 3 φ), with tephra particles being about twice the diameter of bubbles (difference of 1 φ). This correlation appears to be evidence consistent with the dominant role of vesicle bursting, and the slightly smaller size of vesicles compared to pyroclasts probably reflects the fact that many vesicles were not exploded. The Fuego deposit has about 38 vol.% vesicles, which even when corrected for

the crystal content is only about 50 vol.%, well below the 70–80% “packing limit” of Sparks (1978). Because of this it may be that an eruption model that involves degassing during magma ascent and gas loss through permeable subsurface formations (e.g. Sparks et al. 1997, Chapter 3) is operating at Fuego. There also may be more small vesicles in the Fuego magma which gave rise to the finer ash. We note that the observed vesicle sizes in the Fuego fall materials were measured on large lapilli-sized fragments (Table 1) and are larger than the 6–7 φ (8–16 μm) means observed in another subplinian tephra, the 1992 Crater Peak/ Spurr andesite (Gardner et al. 1998). It is significant that these characteristics may be typical of high Al basaltic systems.

Evidence for the operation of other fragmentation mechanisms from the deposits is not so obvious. The size of phenocrysts (Table 1) is mostly in the range of 1–2 φ (dominant range 0.1–0.8 mm) and even though crystals are abundant, effects of crystal liberation and atmospheric fractionation of crystals are not striking. With respect to crystal breakage, we know that Fuego's melt inclusions are very volatile-rich (Rose et al. 1978; Harris and Anderson 1984), so crystal breakage should occur to some degree, and observations by Rose et al. (1980) support this idea. There is no evidence we can see that supports the hydrofracturing mechanism for the 1974 eruption, such as blocky pyroclast shape, high proportions of lithic materials in ejecta, observations of steam explosions, or bimodal size distributions. The eruptions were pulsating, so the possibility of milling is real, but abrasion of pyroclast edges, which might be expected from milling is not observed. It is possible, however, that the small fine mode in the peripheral bimodal tephra samples reflects milling or crystal breakage mechanisms. Fine particle generation through the action of pyroclastic flows was undoubtedly occurring during Fuego's eruption (Stoiber 1974; Davies et al. 1978), but the pyroclastic flows are only a small fraction (estimated to be ~10% of the total; Fig. 14; Table 3) and elutriated fines from them possibly could account for the 4–9% overall proportion of fines in the Fuego fall deposit. Fuego's eruption resembles many others that are described as vulcanian, and Fuego's activity lacks any evidence of hydromagmatic processes (the steep, cone-like geometry also predicated against this).

Total erupted grain size distribution for the October 14, 1974 eruption

Many, if not most, of the recent observed and studied tephra deposits have bimodal-polymodal individual sample size distributions (e.g. Mount St. Helens 1980, Carey and Sigurdsson 1982; El Chichón 1982, Varekamp et al. 1984;

Carey and Sigurdsson 1986; Bonadonna et al. 2002). In contrast, the Soufriere, St. Vincent, 1979 (phreatomagmatic) deposit was thought to have a unimodal size distribution, but this was an a priori assumption (Brazier et al. 1982). Ruapehu 1996 eruptions also shows a mainly unimodal distribution (Bonadonna and Houghton 2005).

The Fuego October 14 tephra deposit studied here (Fig. 17), and probably the Fuego 1971, Cerro Negro 1968 and 1974 tephra deposits (Rose et al. 1973), all have unimodal, relatively coarse, initial populations. Vulcanian eruptions, on the other hand (e.g. Ngauruhoe 1974 and 1975; Self 1975; Nairn et al. 1976), appear to produce deposits much richer in lithic material than the Fuego tephra, but the effect of this on total grain size distribution is not determinable with our available data. One possibility is that confusion about terminology has caused many eruptions to have been termed “vulcanian” when they are actually subplinian, as we infer here for Fuego. However, there are few, if any, well-studied examples of subplinian basaltic eruptions such as the October 14 event available by which to draw more general conclusions. The total grain size distribution estimated here differs strikingly from the 1997 vulcanian Montserrat eruptions studied by Bonadonna et al. (2002). When we compare Fuego tephra with the 1997 vulcanian tephra deposits from Soufriere Hills (SH) Volcano, Montserrat, (Bonadonna et al. 2002), we note that the SH whole-deposit grain-size distribution has much finer ash overall, is strongly bimodal, and these differences probably reflect a much higher contribution from pyroclastic flows. Fuego's whole-deposit size distribution resembles the coarse population of Montserrat.

The basic difference in total grain size distribution of this deposit compared to other types from more silicic eruptions reflects different fragmentation mechanisms controlled by smaller and fewer vesicles and higher proportions of (often larger) crystals than in silicic magma. One notable exception is that of silicic eruptions related to shallow level degassing and lava dome growth. These eruptions also produce vesicle-poor but crystal rich pumice clasts (e.g., Montserrat). Plinian-style activity can be induced by large viscosity increases and secondary pressurization due to substantial gas losses at shallow levels (Sparks et al. 1997), and pyroclastic cones make ideal pathways for gas loss at shallow levels. No evidence suggests a phreatomagmatic influence in the Fuego eruption or deposit. It seems likely that a model similar to that proposed by Druitt et al. (2002) for the vulcanian eruptions of Soufriere Hills, Montserrat, where rapid decompression and brittle fragmentation broke the magma, was also operating in the Fuego case. It could be that abrasion and elutriation in the pyroclastic flows were partly responsible for the finer particles, which are a fine tail on the unimodal

total GSD for Fuego, and which fell out more slowly than most of the deposit.

Tephra dispersal pattern for the October 14, 1974 eruption

The October 14 deposit, sampled virtually over its entire extent, displays some remarkable features:

1. There is no sign of secondary thickening in the bulk deposit thickness data. A priori, two interpretations are possible: either one was produced but was not preserved or a secondary thickening is not expected to have developed for this eruption. As the deposit was sampled so extensively and so rapidly after deposition, the mass deposited beyond the sampled fallout limit must represent only a very small fraction of the total mass erupted. The outer limit of deposition was observed as a sharp one. So it just does not appear that a secondary thickening developed for this eruption. How can this be rationalized?

All cases of secondary thickening reported to date have been for eruptions producing a large amount of fine ash (e.g. MSH Plinian deposit and many others; Brazier et al. 1983). This leads to a decoupling between near-vent fallout of coarse material from the eruption column and fallout of increasingly fine particles from the advected gravity current or umbrella cloud (Ernst 1996). Whether or not a prominent secondary thickening develops in the bulk deposit depends upon several factors and particularly on the coarseness of the total erupted size distribution. For a relatively coarse erupted grainsize distribution and especially for one that has a small spread of sizes around the mean, most of the particles fall from the eruption column or the early advected umbrella cloud and are advected relatively together to the ground, leading to an elongated deposit but not to marked secondary thickening. Secondary thickening is also more pronounced in strong winds and for a higher eruption column as there is more potential to separate out from each other the coarse particles falling from the eruption column from the fine particles advecting with the umbrella cloud (see Ernst 1996).

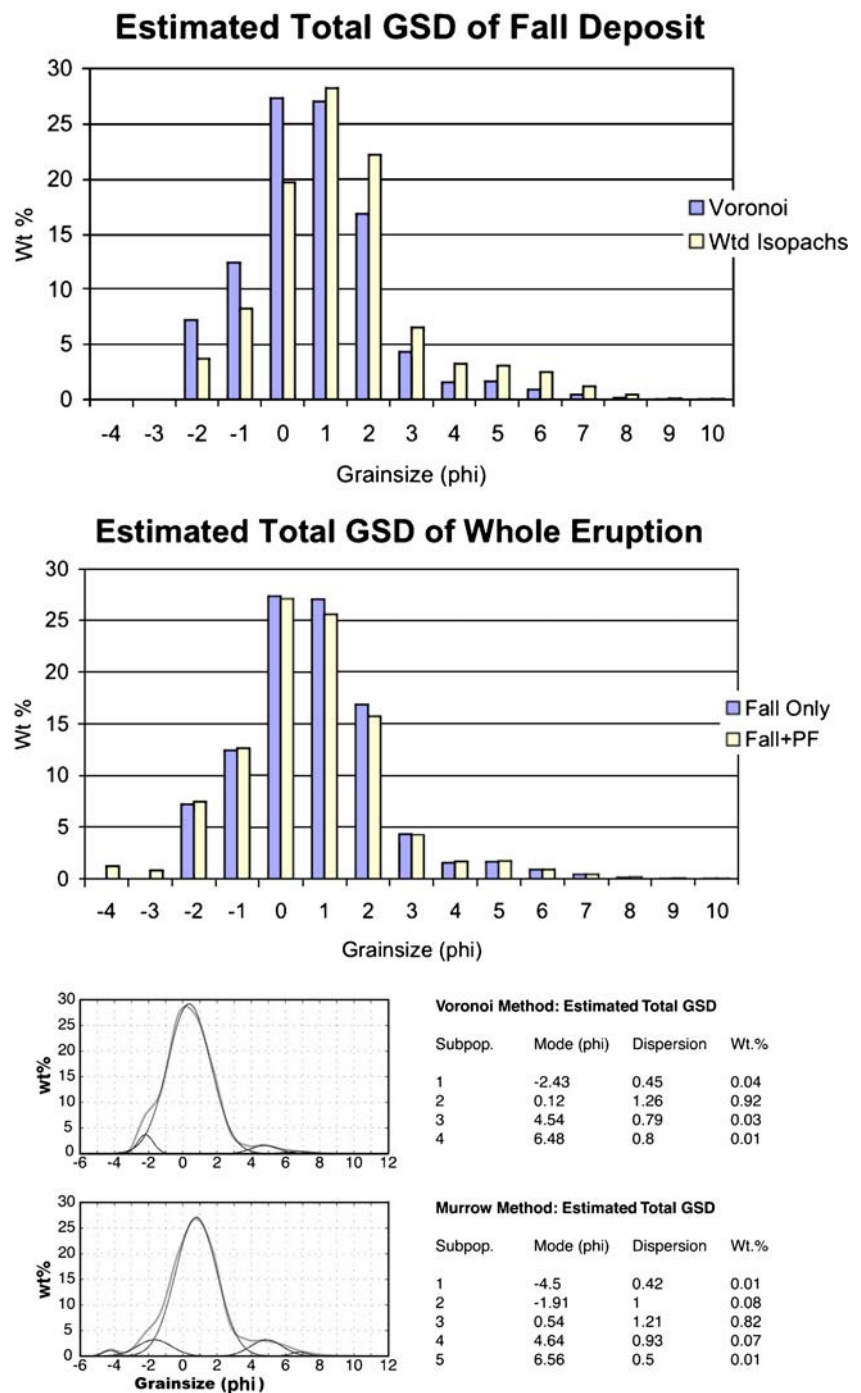
For the Fuego deposit, the reconstructed total grainsize is a fine one for a basaltic eruption but a coarse one for a “Plinian” eruption. In a dispersal diagram, the expectation for a Plinian eruption with broad distribution of erupted sizes is that there will be at least three segments (Bonadonna et al. 1998). The dispersal diagram for the October 14 event is consistent with two segments, with a very steep overall thickness decay away from vent and no third segment. According to Bonadonna et al. (1998), this is consistent with the theoretical expectation for eruption from a relatively low eruption column, of a narrow, coarse initial grainsize distribution (see Fig. 4 a curve 10 and Fig. 6 with

gs3 in Bonadonna et al. 1998). Compared to large eruptions, the Fuego eruption column had a relatively moderate height. Winds were also weak preventing preferential advection of fines to produce a secondary maximum. Altogether, the October 14 event is a type example where secondary thickening (in bulk deposit data terms) is not expected to develop.

2. To our knowledge, it is also the first documented fall deposit to display a bimodal-unimodal-bimodal pattern of grainsize distributions across the dispersal axis, superimposed on a thickness dispersal pattern corresponding to a relatively simple “elliptical” fan. How can this combination be rationalized?

Ernst et al. (1994) studied experimentally the interaction between an eruption column and a crosswind for contrasting plume-to-crossflow strength ratios. For the eruption of a strong plume becoming distorted and bent-over only as it approaches its final rise height, in weak crosswind, and under the influence of a strong density interface (tropopause), optimal conditions are present for partitioning the ascending flow into two regimes of flow that closely overlap each other. On the one hand, most of the flow is trying to flow radially at the final rise height, giving rise to a dominant advected gravity current (Figs. 2 a, b in Ernst et al. 1994). On the other hand, a smaller part of the flow bifurcates to form two counter-spiralling eddies spreading immediately underneath the advected gravity current. In the case of Fuego, partitioning of most of the ascending flow into an advected gravity current can account for the thickness decay pattern, isopach map pattern, for the unimodal grainsize distributions and overall decrease in grainsize along the dispersal axis. Partitioning of a smaller fraction of the fluid into a bifurcating plume, however, needs to be invoked to most readily account for the bimodal character at the N and S edges of the deposit. How can such a pattern be explained? As this bifurcating flow is dynamically weaker, it will mostly disperse the finer grainsizes, the coarser grainsizes being carried by the more powerful central flow that will give rise to the advected gravity current. In a bifurcating plume, there is strong circulation with vigorous entrainment of air and reentrainment of the finer fraction falling in the region bisecting the two plume lobes. As these fine particles circulate, interact with each other and with moisture, condensed water or ice, they will form mixed particle aggregates which will tend to fall on the downwelling outer edges of the counter-spiralling eddies, where reentrainment is also much less likely. These aggregates can mainly form from the fine ash mode ($\sim 4.5 \varphi$ or $44 \mu\text{m}$) (Figs. 10, 11, 12), which is volumetrically minor in this eruption, the other particles larger than 100 microns being unfavourable for aggregation. Thus in the Fuego case, falling fine ash as single

Fig. 17 Comparison of various estimates of total grain size distribution of Fuego’s October 14, 1974, erupted particles. Voronoi set is done following the method of Bonadonna and Houghton (2005) while the other method is based on weighted proportions of isopach regions (Murrow et al. 1980). The plot above compares the two methods of estimating the total GSD for the fall deposit alone. Note that the Voronoi method yields a coarser grain size overall, by about one ϕ . The lower plot compares the GSD of the fall deposit alone with the whole eruption GSD, which includes a 10% mass of block-and-ash flow deposit, which are not part of the tephra fall. At right are deconvolutions of lognormal modes, as in Fig. 12, for the total GSDs (see text for discussion)



particles or as aggregates would only add moderately to the main dispersal fan (from eruption column fall or advected gravity current) and mostly at the edges of the deposition fan. Altogether, this would then lead to the bimodal-unimodal-bimodal grainsize dispersal pattern measured for the Fuego deposit. Such a pattern is expected for subplinian, tropopause-height, explosive eruptions, but had not previously been documented.

There is a certain degree of asymmetry in the bimodal-unimodal-bimodal dispersal pattern and this can

readily be accounted for in conditions of veering wind direction and changing speeds reported in the Fuego region on October 14. Veering winds will strengthen one of the counter-spiralling eddies preferentially and will lead to asymmetric bifurcation with a higher and a lower plume lobe spreading downwind at different speeds (see Ernst et al. 1994).

In summary, the finest ash ($< 8 \mu\text{m}$) is only found in considerable proportions at the very edge of the tephra deposit (Fig. 12; samples 200, 252). Awareness of the

serious health hazards of fine ash is growing (e.g. Bernstein et al. 1986; Buist et al. 1986; Baxter et al. 1999), and the possible association of concentrations of fine ash with milling by pyroclastic flows is notable.

Significance of subplinian tephra deposits

Walker (1973) suggested that vulcanian deposits occupy a wide field on the Dispersal (D) vs. Fragmentation (F) classification scheme, and Wright et al. (1980; Fig. 4, p. 322) demonstrated this by plotting several vulcanian tephra deposits. Some vulcanian deposits plot on the D vs F diagram at a very high F value (in the phreatoplinian field), reflecting that the deposits are dominated by grain sizes < 1 mm, but they are not as fine-grained as phreatomagmatic deposits or as co-PF-rich deposits, such as MSH 1980. On a plot of thickness versus square root of area, the Fuego tephra deposit resembles smaller Plinian deposits (Fig. 15). This result confirms our earlier assertion (see Background, paragraph 1) that it is an example of a basaltic subplinian eruption.

Many vulcanian and subplinian tephra deposits are insignificant in the geological record, yet eruptions of this style occur frequently worldwide. As shown here, and by many other examples, the deposits are only moderately widespread, and generally fine-grained and thin even though they are commonly dispersed from stratosphere-high eruption columns. Together with the propensity for basaltic-andesitic magmas to be more inherently sulfur-rich than silicic melts, there is a reason why subplinian and vulcanian eruptions and their tephra deposits should be more closely studied in future, besides the most obvious hazards aspects. Vulcanian and subplinian events are the most frequent to vent particles, gas, and acid aerosols to the upper atmosphere, and are expected to be instrumental in controlling the background stratospheric aerosol level. A small series of events from Fuego 1974, caused a measurable stratospheric impact (Hoffman and Rosen 1977). Slightly larger but similar events, such as Agung 1963, caused small but measurable climate change (Newell 1970; Rampino and Self 1984). The Montserrat eruptions were generally shorter lived and smaller so they had limited atmospheric effects. Yet these eruptions will have no long term record in tephra sequences, and a corollary of this is that unless the eruptive history of a volcano is intimately known, as is the case for Fuego since A.D. 1800 (Martin and Rose 1981), determining post facto that an eruption of possible atmospheric significance took place is virtually impossible. If we bear this in mind, together with the potential atmospheric impact of even modest vulcanian and subplinian events, it may change our perspective of the importance of these common eruptions.

Conclusions

The October 14 tephra fall deposit of the Fuego 1974 eruptive sequence was a high-Al basalt scoria ash and lapilli deposit produced by a subplinian eruption, with a pulsating gas thrust but a maintained moderately “strong plume”. In a period of at least 5 h, 0.02 km³ (DRE) of material was ejected, forming an eruption column with a maximum height of about 15 km asl. The base of the spreading volcanic cloud was at about 13 km asl and an upper tropospheric ENE wind dispersed the ejecta to form a coherent fall unit out to 70 km downwind. The tephra fall deposit is dominated by scoria lapilli and ash with a unimodal size distribution showing a regular decrease in size downwind. Only in the marginal areas, and in distal samples, is there a substantial (> 10 wt%) fine ash mode, giving a bimodal size distribution. The best explanation of this fine-grained material is that it was created by the milling of block-and-ash flows which descended Fuego’s slopes during the eruption. These hot block-and-ash flows elutriated fine-grained ash to form an ash cloud above the avalanche. The co-PF ashcloud was then either dispersed in a slightly different direction (WNW) than the coarser ash which was erupted to a high altitude where winds were stronger and to the WSW, or it merged with a rising eruption column interacting increasingly strongly with crosswinds during ascent and ultimately dispersing in the form of a dominant advected current and underlying bifurcating plume flow. Fine ash was present where coarse ashfall fell through the lower, finer elutriated cloud and where fine ash particles were captured and/or aggregated in the moist atmosphere. Alternatively the deposit may result from two overlapping deposits, the fine ash falling dominantly from the bifurcating flow edges and all coarser sizes falling from the more vertical eruption column and advected current. An estimate of the total grain size distribution of the October 14 ejecta, whether or not it includes the pyroclastic flow deposit, yields a relatively coarse and unimodal initial population. This contrasts strongly with fines-dominated, polymodal initial populations estimated for many recent and historic tephra deposits of other eruptive styles, both Plinian and phreatomagmatic, but it is in agreement with the total grain size distribution of the tephra deposit produced by the subplinian eruption of Ruapehu 1996.

We propose that the October 14, 1974, tephra deposit from Fuego is fairly typical of fine-grained, generally thin, and short-lived, tephra deposits commonly produced by the dry subplinian eruptions of many composite volcanoes. Similar characteristics are shown by the 1971 Fuego tephra fall deposit, and tephra deposits from Cerro Negro volcano in Nicaragua. Deposits like Fuego’s are not well preserved in the geologic record, but are common and could represent

a significant part of the erupted materials for some volcanoes. Health hazards of these deposits include significant amounts of ash finer than 10 μm diameter, apparently derived from milling of block and ash flows and which may be distributed by lower level winds or by fallout from the edges of a portion of the flow which bifurcates underneath the dominant advected current.

Acknowledgements Once again, Samuel B. Bonis is gratefully acknowledged for his sample collection prowess. Jocelyn McPhie, Jacqueline Huntoon and two anonymous reviewers helped to clarify the text and figures. We thank the technical staff at the Institute of Materials Processing, MTU, for their help in Coulter counter analysis. WIR was supported by NSF and NASA. SS received support from NASA grant NSG5131 for the study of atmospheric effects of volcanic eruptions. GGJE was helped by interactions with RSJ Sparks, J Willson, and C Bonadonna, and support from the Nuffield Foundation (NUF-NAL award). The University of Cambridge Physical Geography Laboratories generously allowed AJD use of the Malvern Room facility; in particular Claire Horwell, Steve Boreham and Chris Rolfe are thanked for their assistance and support.

References

- Anderson AT Jr. (1984) Probable relations between plagioclase zoning and magma dynamics, Fuego Volcano, Guatemala. *Amer Mineral* 69(7–8):660–676
- Andres RJ, Rose WI, Stoiber RE, Williams SN, Matías O, Morales R (1993) A summary of sulfur dioxide emission rate measurements from Guatemalan volcanoes. *Bull Volcanol* 55:379–388
- Baxter PJ (1999) Cristobalite in volcanic ash of the Soufrière Hills Volcano, Montserrat: hazards implications. *Science* 283:1142–1145
- Bernstein RS, Baxter PJ, Falk H, Ing R, Foster L, Frost F (1986) Immediate health concerns and actions in volcanic eruptions: lesson from the Mount St Helens eruptions, May 18–October 18, 1980. *Am J Public Health* 76(suppl):25–37
- Bonadonna C, Houghton B (2005) Total grain size distribution and volume of tephra-fall deposits. *Bull Volcanol* 67:441–456
- Bonadonna C, Ernst GGJ, Sparks RSJ (1998) Thickness variations and volume estimates of tephra fall deposits: the importance of particle Reynolds number. *J Volcanol Geotherm Res* 81:173–184
- Bonadonna C, Mayberry GC, Calder ES, Sparks RSJ, Choux C, Jackson, P, Lejeune AM, Loughlin SC, Norton GE, Rose WI, Ryan G, Young SR (2002) Tephra fallout in the eruption of Soufrière Hills Volcano, Montserrat. In: Druitt TH, Kokelaar BP (eds) *The eruption of Soufrière Hills Volcano, Montserrat, from 1995 to 1999*. *Geol Soc London Mem* 21:483–516
- Brazier S, Davis AN, Sigurdsson H, Sparks RSJ (1982) Fallout and deposition of volcanic ash during the 1979 explosive eruption of the Soufrière of St. Vincent. *J Volcanol Geotherm Res* 144:335–359
- Brazier S, Sparks RSJ, Carey SN, Sigurdsson H, Westgate JA (1983) Bimodal grain size distribution and secondary thickening in air-fall ash layers. *Nature* 301:115–119
- Buist AS, Martin TR, Short JH, Butler J, Lybarger JA (1986) The development of a multidisciplinary plan for evaluation of long-term health effects of the Mount St Helens eruptions. *Am J Public Health* 76(suppl):39–44
- Carey SN, Sigurdsson H (1982) Influence of particle aggregation on deposition of distal tephra from the May 18, 1980, eruption of Mount St. Helens volcano. *J Geophys Res* 87:7061–7072
- Carey SN, Sigurdsson H (1986) The 1982 eruptions of El Chichón volcano, Mexico (2): Observations and numerical modelling of tephra-fall distribution. *Bull Volcanol* 48:127–142
- Carey SN, Sparks RSJ (1986) Quantitative models of the fall out and dispersal of tephra from volcanic eruption columns. *Bull Volcanol* 48:109–126
- Carr MJ, Rose WI (1987) CENTAM—a data base of Central American volcanic rocks. *J Volcanol Geotherm Res* 33(Stoiber Volume):239–240
- Cas RAF, Wright JV (1987) *Volcanic successions: modern and ancient*. Unwin Hyman, London
- Chesner CA, Rose WI (1984) Geochemistry and evolution of the Fuego volcanic complex, Guatemala. *J Volcanol Geotherm Res* 21:25–44
- Chesner CA, Halsor SP (1997) Geochemical trends of sequential lava flows from Meseta volcano, Guatemala. *J Volcanol Geotherm Res* 78:221–237
- Cioni R, Marianelli P, Santacroce R, Sbrana A (2000) Plinian and Subplinian eruptions. In: Sigurdsson H (ed) *Encyclopedia of Volcanoes*. Academic, San Diego, pp 477–495
- Davies DK, Quearry MW, Bonis SB (1978) Glowing avalanches from the 1974 eruption of the volcano Fuego, Guatemala. *Geol Soc Amer Bull* 89:369–384
- Draxler RR, Hess GD (1998) An overview of the Hysplit 4 modeling system for trajectories, dispersion and deposition. *Aust Meteorol Mag* 47:295–308
- Druitt TH, Young SR, Baptie B, Bonadonna C, Calder ES, Clarke AB, Cole PD, Harford CL, Herd RA, Luckett R, Ryan G, Voight B (2002) Episodes of repetitive Vulcanian explosions and fountain collapse at Soufrière Hills Volcano, Montserrat. In: Druitt TH, Kokelaar BP (eds) *The eruption of Soufrière Hills Volcano, Montserrat, from 1995 to 1999*. *Geol Soc London, Mem* 21:
- Ernst GGJ (1996) *Dynamics of sediment-laden plumes*. Ph D Thesis, U Bristol, UK
- Ernst GGJ, Davis JP, Sparks RSJ (1994) Bifurcation of volcanic plumes in a crosswind. *Bull Volcanol* 65:159–169
- Fisher RV, Schmincke H-U (1983) *Pyroclastic rocks*. Springer-Verlag, Berlin
- Freundt A, Wilson CJN, Carey SN (2000) Ignimbrites and block-and-ash flow deposits. In: Sigurdsson H (ed) *Encyclopedia of Volcanology*. Academic, San Diego, pp 581–599
- Gardner CA, Cashman KV, Neal CA (1998) Tephra fall deposits from the 1992 eruption of Crater Peak, Alaska: implications of clast textures for eruptive products. *Bull Volcanol* 59:537–555
- Gardner JE, Thomas RME, Jaupart C, Tait S (1996) Fragmentation of magma during Plinian volcanic eruptions. *Bull Volcanol* 58:144–162
- Harris DM, Anderson AT (1984) Volatiles H₂O, CO₂, and Cl in a subduction related basalt. *Contrib Mineral Petrol* 87(2):120–128
- Herzog M, Graf HF, Textor C, Oberhuber JM (1998) The effect of phase changes of water on the development of volcanic plumes. *J Volcanol Geotherm Res* 87:55–74
- Hildreth W, Drake RE (1992) Volcán Quizapu, Chilean Andes. *Bull Volcanol* 54:93–125
- Hoffman DJ, Rosen JM (1977) Balloon observations of the time development of the stratospheric aerosol event of 1974–75. *J Geophys Res* 82:1435–1440
- Huang TC, Watkins ND, Shaw DM (1975) Atmospherically transported volcanic glass in deep-sea sediments: development of a separation and counting technique. *Deep-Sea Res* 22:185–196
- Inman DL (1952) Measures of describing the size distribution of sediments. *J Sediment Petrol* 22:125–145
- Keller J (1980) The island of Vulcano. *Soc Italiana Min Petr* 36:368–413
- Krotkov NA, Torres O, Sefor C, Krueger AJ, Kostinski A, Rose WI, Bluth GJS, Schneider DJ, Shaefer SJ (1998) Comparison of TOMS and AVHRR volcanic ash retrievals from the

- August 1992 eruption of Mount Spurr. *Geophys Res Lett* 26: 455–458
- Lazrus AL, Cadle RD, Gandrud BW, Greenberg JP, Huebert BJ, Rose WI (1979) Sulfur and halogen chemistry of the stratosphere and of volcanic eruption plumes. *J Geophys Res* 84:7869–7875
- LeBas MJ, LeMaitre RW, Streckeisens AL, Zanetin B (1986) A chemical classification of volcanic rocks based on the alkali-silica diagram. *J Petrol* 27:745–750
- Martin DP, Rose WI (1981) Behavior patterns of Fuego volcano, Guatemala. *J Volcanol Geotherm Res* 10:67–81
- McBirney AR (1973) Factors governing the intensity of andesitic eruptions. *Bull Volcanol* 37:443–453
- McCormick MP et al (1978) Post-volcanic stratospheric aerosol decay as measured by Lidar. *J Atmos Sci* 35:1296–1305
- Meinel AB, Meinel MP (1975) Stratospheric dust-aerosol event of November 1974. *Science* 188:477–478
- Morrissey MM, Mastin LG (2000) Vulcanian eruptions. In: Sigurdsson H (ed) *Encyclopedia of Volcanoes*. Academic, San Diego, pp 463–476
- Murrow PJ, Rose WI, Self S (1980) Determination of the total grain size distribution in a vulcanian eruption column, and its implications to stratospheric aerosol perturbation. *Geophys Res Lett* 7:893–896
- Nairn IA, Hewson CAY, Latter JH, Wood CP (1976) Pyroclastic eruptions of Ngauruhoe Volcano, central North Island, New Zealand, 1974 January and March. In: Johnson RW (ed) *Volcanism in Australasia*. Elsevier, Amsterdam, pp 385–405
- Nairn IA, Self S (1978) Explosive eruptions and pyroclastic avalanches from Ngauruhoe in February 1975. *J Volcanol Geotherm Res* 3:39–60
- Neal CA, McGimsey RG, Gardner CA, Harbin ML, Nye CJ (1994) Tephra fall deposits from the 1992 eruptions of Crater Peak, Mount Spurr Volcano, Alaska: a preliminary report on distribution, stratigraphy and composition. *U S G S Bulletin* 2139: 65–79
- Newell RE (1970) Stratospheric temperature change from the Mt. Agung volcanic eruption of 1963. *J Atmos Sci* 27:977–978
- Pyle DM (1989) The thickness, volume and grainsize of tephra fall deposits. *Bull Volcanol* 51:1–15
- Pyle DM (1990) New estimates for the volume of the Minoan eruption. In *Thera and the Aegean World III*. Proceedings of the Third International Congress, Santorini, Greece, 3–9 September 1989, Vol 2, pp 113–121
- Rampino R, Self S (1984) Sulphur-rich volcanic eruptions and stratospheric aerosols. *Nature* 310:677–679
- Riley CM, Rose WI, Bluth GJS (2003) Quantitative shape measurements of distal volcanic ash. *Jour Geophys Res* 108, no B10-2504 DOI 10.1029/2001JB000818
- Roggensack K (2001) Unraveling the 1974 eruption of Fuego Volcano (Guatemala) with small crystals and their young melt inclusions. *Geology* 29(10):911–914
- Rose WI (1977) Scavenging of volcanic aerosol by ash: atmospheric and volcanologic implications. *Geology* 5:621–624
- Rose WI, Anderson AT, Woodruff LG, Bonis SB (1978) The October 1974 basaltic tephra from Fuego volcano: description and history of the magma body. *J Volcanol Geotherm Res* 4:3–53
- Rose WI, Bluth GJS, Schneider DJ, Ernst GGJ, Riley CM, McGimsey RG (2001) Observations of 1992 Crater Peak/Spurr Volcanic Clouds in their first few days of atmospheric residence. *J Geology* 109:677–694
- Rose WI, Bonis S, Stoiber RE, Keller M, Bickford T (1973) Studies of volcanic ash from two recent Central American eruptions. *Bull Volcanol* 37:338–364
- Rose WI, Chuan RL, Cadle RD, Woods DC (1980) Small particles in volcanic eruption clouds. *Amer Jour Sci* 280:671–696
- Rose WI, Delene DJ, Schneider DJ, Bluth GJS, Krueger AJ, Sprod I, McKee C, Davies HL, Ernst GGJ (1995) Ice in the 1994 Rabaul eruption cloud: implications for volcano hazard and atmospheric effects. *Nature* 375:477–479
- Rose WI, Wunderman RL, Hoffman MF, Gale L (1983) A volcanologist's review of atmospheric hazards of volcanic activity: Fuego and Mount St. Helens. *J Volcanol Geotherm Res* 17:133–157
- Rose WI, Stoiber RE, Malinconico LL (1982) Eruptive gas compositions and fluxes of explosive volcanoes; budget of S and Cl emitted from Fuego Volcano, Guatemala. In: Thorpe RS (ed) *Andesites: Orogenic Andesites and Related Rocks*. Wiley & Sons, Chichester, United Kingdom, pp 669–676
- Sarna-Wojcicki AM, Shipley S, Waitt RB, Dzurisin D, Wood SH (1981) Areal distribution, thickness, mass, volume and grain size of air-fall ash from the six major eruptions of 1980. *US Geol Surv Prof Paper* 1250:667–681
- Scasso RA, Corbella H, Tiberi P (1994) Sedimentological analysis of the tephra from the 12–15 August 1991 eruption of Hudson Volcano. *Bull Volcanol* 56:121–132
- Schneider DJ, Rose WI, Coke LR, Bluth GJS, Sprod I, Krueger AJ (1999) Early evolution of a stratospheric volcanic eruption cloud as observed with TOMS and AVHRR. *J Geophys Res* 104:4037–4050
- Self S (1975) Explosive activity of Ngauruhoe, 27–30 March 1974. *NZ J Geol Geophys* 18:189–195
- Sisson TW, Layne GD (1993) H₂O in basalt and basaltic andesite glass inclusions from four subduction-related volcanoes. *Earth Planet Sci Lett* 117:619–635
- Sparks RSJ (1978) The dynamics of bubble formation and growth in magmas—a review and analysis. *J Volcanol Geotherm Res* 3:1–37
- Sparks RSJ (1997) Causes and consequences of pressurization in lava dome eruptions. *Earth Planet Sci Lett* 150:177–189
- Sparks RSJ, Bursik MI, Carey SN, Gilbert JS, Glaze LS, Sigurdsson H, Woods AW (1997) *Volcanic plumes*. Wiley & Sons, Chichester
- Sparks RSJ, Walker GPL (1977) The significance of vitric-enriched airfall ashes associated with crystal enriched ignimbrites. *J Volcanol Geotherm Res* 2:329–341
- Sparks RSJ, Wilson L, Sigurdsson H (1981) The pyroclastic deposits of ? the 1875 eruption of Askja, Iceland. *Phil Trans Roy Soc London* 299:241–273
- Stoiber RE (1974) Eruption of Volcan Fuego—October 14, 1974. *Bull Volcanol* 38:861–869
- Textor C, Graf HF, Herzog M, Oberhuber JM, Rose WI, Ernst GGJ (2006a) Volcanic particle aggregation in explosive eruption columns. Part I: Parameterization of the microphysics of hydrometeors and ash. *J Volcanol Geotherm Res* 150:359–377
- Textor C, Graf HF, Herzog M, Oberhuber JM, Rose WI, Ernst GGJ (2006b) Volcanic particle aggregation in explosive eruption columns. Part II: Numerical Experiments. *J Volcanol Geoth Res* 150:378–394
- Vallance JW, Siebert L, Rose WI, Giron JR, Banks NG (1995) Edifice collapse and related hazards in Guatemala. *J Volcanol Geotherm Res* 66:337–355
- Varekamp JC, Luhr JF, Prestegard KL (1984) The 1982 eruptions of El Chichón Volcano, Chiapas, Mexico: mineralogy and petrology of the anhydrite-bearing pumices. *J Volcanol Geotherm Res* 23:39–68
- Volz FE (1975) Volcanic twilights from the Fuego eruption. *Science* 189:48–50
- Wadge G (1980) *Output rate of magma from active central volcanoes*. Macmillan Journals, London, United Kingdom
- Walker GPL (1981) Characteristics of two phreatoplinitic ashes, and their water-flushed origin. *J Volcanol Geotherm Res* 9:395–407
- Walker GPL (1973) Explosive volcanic eruptions—a new classification scheme. *Geol Rundsch* 62:431–446

- Walker GPL (1980) The Taupo pumice: product of the most powerful known (ultraplinian) eruption. *J Volcanol Geotherm Res* 8:69–94
- Walker GPL (1981b) Generation and dispersal of fine ash and dust by volcanic eruptions. *J Volcanol Geotherm Res* 11:81–94
- Walker GPL (1982) Eruptions of andesitic volcanoes. In: Thorpe RS (ed) *Andesites*. Wiley & Sons, New York, pp 403–413
- Walker GPL, Self S, Wilson L (1984) Tarawera 1886, New Zealand—a basalticPlinian fissure eruption. *J Volcanol Geotherm Res* 21: 61–78
- Wen S, Rose WI (1994) Retrieval of particle sizes and masses in volcanic clouds using AVHRR bands 4 and 5. *J Geophys Res* 99: 5421–5431
- Wilson L, Huang TC (1979) The influence of shape on the atmospheric settling velocity of volcanic ash particles. *Earth Planet Sci Lett* 44:311–324
- Wohletz KH, Sheridan MF, Brown WK (1989) Particle size distributions and the sequential fragmentation/transport theory applied to volcanic ash. *J Geophys Res* 94:15703–15721
- Wright JV, Smith AL, Self S (1980) A working terminology of pyroclastic deposits. *J Volcanol Geotherm Res* 8:315–336
- Young SR, Sparks RSJ, Aspinall WP, Lynch LL, Miller AD, Robinson REA, Shepherd JP (1998) Overview of the eruption of Soufrière Hills Volcano, Montserrat, July 18, 1995 to December 1997. *Geophys Res Lett* 25:3389–3392